Epilepsia, 47(6):991–997, 2006
Blackwell Publishing, Inc.

Magnetoencephalography in Patients with Tuberous Sclerosis and Localization-related Epilepsy

*†Takanori Kamimura, †Jun Tohyama, ‡Makoto Oishi, †Noriyuki Akasaka, †Osamu Kanazawa, §Mutsuo Sasagawa, ||Mitsuhiro Kato, ¶Kousaku Ohno, ‡Hiroshi Masuda, ‡Shigeki Kameyama, and *Makoto Uchiyama

**Division of Pediatrics, Department of Homeostatic Regulation and Development, Course for Biological Functions and Medical Control, Niigata Graduate School of Medical and Dental Sciences, and Departments of †Pediatric Neurology, ‡Neurosurgery, and §Psychiatry, Epilepsy Center, Nishi-Niigata Chuo National Hospital, Niigata; ||Department of Pediatrics, Yamagata University School of Medicine, Yamagata; and ¶Division of Child Neurology, Institute of Neurological Sciences, Faculty of Medicine, Tottori University, Yonago, Japan*

Summary: *Purpose:* To clarify the usefulness of magnetoencephalography (MEG) for diagnosis of the spatial relations between spike foci and suspicious epileptogenic tubers on MRI in patients with tuberous sclerosis (TS) and to compare MEG spike foci with single-photon emission computed tomography (SPECT) findings.

Methods: We analyzed magnetic fields of epileptic spike discharges in 15 patients with TS and localization-related epilepsy (LRE) by using MEG (a whole-head 204-channel magnetometer system). We investigated the spatial relation between the equivalent current dipoles (ECDs) of interictal spike discharges and visible cortical tubers on MRI. We also compared results of MEG and MRI with SPECT findings.

Results: MEG detected a cluster of ECDs around one cortical tuber in six of 15 patients and clusters of ECDs around two cortical tubers in five patients. Interictal SPECT was disappointing in detection of epileptic foci in TS. However, MEG spike foci showed spatial consistency with ictal hyperperfusion areas in two patients. Three patients with single ECD clusters underwent surgical treatment: two have been seizure free, and one has obtained seizure reduction of >90%.

Conclusions: ECDs were located around visible tuber nodules. MEG enabled precise localization of the epileptic foci and provided crucial information for surgical treatment in patients with TS and partial epilepsy. TS patients showing a single ECD cluster on MEG may be appropriate candidates for surgical treatment. **Key Words**: Tuberous sclerosis—Symptomatic localization-related epilepsy—Magnetoencephalography—SPECT—Epileptic focus.

Tuberous sclerosis (TS) is a multisystem disorder of tissue growth and differentiation characterized by tumors in the brain, eyes, heart, and kidneys, and by cutaneous abnormalities (1,2). TS is inherited as an autosomal dominant trait with high penetrance and variable expressivity. However, about two thirds of TS cases are sporadic, resulting from spontaneous genetic mutations in the offspring of healthy parents (1,3). Mutations or deletions of two separate genes, *TSC1* and *TCS2*, have been identified in patients with TS (3).

One of the most important complications of TS is epilepsy. Infantile spasms are the most common type of seizure at presentation (4). Partial seizures are often seen, whereas generalized seizures are relatively rare (1,4). Epileptic foci are generally restricted to a limited cortical area, even when multiple cortical tubers are present (5,6). Several authors reported that surgical treatment of patients with TS and intractable epilepsy is most effective if a single tuber or true epileptic foci can be identified as the source of seizures and resected. (5–8). In the presence of multiple cortical tubers, preoperative evaluation with multiple modalities such as scalp video-EEG monitoring, positron emission tomography, single-photon emission computed tomography (SPECT), and magnetoencephalography (MEG) is considered necessary for the accurate identification of true epileptic foci. However, only a few reports on evaluation of MEG in TS patients have been published (9,10). These studies did not use a whole-head magnetometer for evaluating ECDs, and no MEG studies have been preformed with a large number of TS patients. The aims of the present study were to clarify the usefulness of the whole-head MEG system in determining the spatial relation between the MEG spike

Accepted November 30, 2005.
Address correspondence and reprint requests to Dr. J. Tohyama at Department of Pediatric Neurology, Epilepsy Center, Nishi-Niigata Chuo National Hospital, Masago 1-14-1, Niigata 950-2085, Japan. E-mail: jtohyama@masa.go.jp

foci and suggestive epileptogenic tubers on MRI and to compare MEG spike foci with SPECT findings for the diagnosis of epileptic foci in patients with TS.

METHODS

Patients

From all patients who attended the Epilepsy Center, Nishi-Niigata Chuo National Hospital between January 2000 and March 2005, 15 patients diagnosed with both TS and localization-related epilepsy (LRE) (seven male and eight female patients, age 2–40 years; mean, 15.1 years) were selected (Table 1). TS was diagnosed on the basis of skin lesions and multiple cortical tubers on MRI that exhibited calcification on computed tomography (CT), whereas symptomatic LRE (SLRE) was diagnosed according to criteria of the International Classification of Epilepsies and Epileptic Syndromes (11). In two patients (cases 2 and 13), mutations of *TSC1* and *TSC2* were investigated with polymerase chain reaction (PCR)-single-strand conformational polymorphism (SSCP) and sequencing analysis by using DNA from peripheral leukocytes, confirming the clinical diagnosis. A missense mutation of 4952A>G (N1651S) was found in *TSC2* in case 2, and a nonsense mutation of 3355C>G (Q1119X) was found in *TSC2* in case 13; both mutations were heterozygous. All patients experienced complex partial seizures (CPSs); one patient (case 3) also had secondarily generalized tonic–clonic seizures. Five patients had daily seizures (cases 1, 2, 7, 10, and 14), six had weekly seizures (cases 3, 4, 5, 6, 11, and 12), and four had monthly seizures (cases 8, 9, 13, and 15). Five patients had a history of West syndrome (cases 1, 4, 8, 11, and 13), and three of these five patients had received adrenocorticotropic hormone (ACTH) therapy (cases 4, 11 and 13). All patients had intractable seizures, and various antiepileptic drugs (AEDs) were administered for treatment (Table 1). Tailored-focus resection was performed in three patients (cases 2, 4, and 7).

All 15 patients underwent MRI, MEG, and interictal SPECT. Cases 1, 2, 8, and 13 were sedated because they were too young to cooperate with examinations. The remaining patients remained conscious during examinations. In two cases (cases 2 and 7), ictal SPECT was successfully obtained in addition to interictal SPECT. We also compared localization of the ictal hyperperfusion area with the MEG spike foci.

MRI

To detect epileptogenic lesions, T_1-weighted (T_1-W), T_2-weighted, proton-density weighted (PDW), and fluid-attenuated inversion recovery (FLAIR) MR images were routinely taken with a 1.5-Tesla system (MAGNEX Epios15; Shimadzu, Kyoto, Japan). Both PDW and FLAIR MR were more sensitive for determining the precise location and extent of cortical tubers in each TS patient. We compared localization of cortical tubers on PDW and FLAIR MR images with clusters of ECDs demonstrated by MEG on T_1-W MR images.

MEG

MEG was performed with a whole-scalp neuromagnetometer (Neuromag 204; Elekta-Neuromag, Oy, Finland) in a magnetically shielded room. This device uses 204 planar-type, first-order gradiometers. Before recording, for data reference, we digitized the positions of three anthropometric points (nasion and bilateral preauricular points) and four indicator coils on the scalp with a three-dimensional electromagnetic digitizer (Polhemus, Colchester, VT, U.S.A.). MEG recordings were analyzed with a band-pass filter between 3 and 45 Hz. We analyzed the amplitude of MEG spikes at the MEG sensor location with the highest amplitude. For each MEG spike, we calculated the single ECD source at the initial spike peak with a spherical model. ECD spike sources with goodness-of-fit (GOF) >80% were accepted as valid. Of 204 MEG sensors, we used data from 40 neighboring sensors that encompassed both extremes of the magnetic flux distribution associated with each event. We evaluated dipole moments of the MEG spike sources and overlaid the spike sources onto T_1-W MR images of the patient's head with respect to the three morphometric points. MRI was performed with a 1.5-Tesla system, as described earlier.

SPECT

After the intravenous injection of 600 mBq of ^{99m}Tc-ethyl cysteinate dimer (^{99m}Tc-ECD) for adults, or 600 × (body weight/60)$^{2/3}$ mBq of ^{99m}Tc-ECD for children, SPECT imaging was performed with a PRISM 2000XP (Shimadzu, Kyoto, Japan). A series of 12-mm contiguous slices perpendicular to the orbitomeatal line were obtained for each patient. Ictal scans were obtained by promptly injecting the tracer through a preplaced venous line at the onset of electroclinical seizure detected by continuous video-EEG recording. In one patient, an ictal scan was evaluated by using three-dimensional stereotactic surface projections (3D-SSP) (12) and subtraction ictal SPECT coregistered to MRI (SISCOM) (13) as described.

Surgical treatment

After therapeutic evaluation, three of the 15 patients underwent surgical treatment. As part of the preoperative evaluation, long-term electrocorticography (ECoG) was performed to localize the seizure focus precisely in cases 4 and 7; this was facilitated by implantation of subdural electrodes according to MEG and SPECT results. Case 2 was too young for the implantation of subdural electrodes to be attempted. Localization of resection was decided according to the results of scalp video-EEG, MEG, ictal SPECT, and intraoperative ECoG. All patients underwent tailored-focus resection in addition to tuberectomy.

TABLE 1. *Clinical characteristics and results of investigations for fifteen study patients*

Patient	Sex	Age (yr)	Epilepsy type	Type of seizure	Seizure frequency	Major tubers on MRI	ECDs on MEG	Hypoperfusion on interictal SPECT	Hyperperfusion on ictal SPECT	AED
1	F	2	WS→LRE	CPS	Daily	Lt Fr	Lt Fr	None	n.d.	VPA, CLB, ZNS, PHT, PRM, CZP, SLT, CBZ, KBr, ACZ
2	M	2	LRE	CPS→sGTC	Daily	Lt Fr[a], Lt O[a]	Lt P	Lt Fr,P	Lt P	PHT, VPA, PRM, CBZ, ZNS, CZP, PB
3	M	15	LRE	CPS	Weekly	Rt F	Rt T	Bil Fr,P	n.d.	VPA, CBZ, CZP, PHT
4	M	24	WS→LRE	CPS	Weekly	Rt Fr[a], Lt Fr	Rt Fr	Bil Fr	n.d.	CBZ, ZNS, VPA, PHT, CZP, CLB
5	F	25	LRE	CPS	Weekly	Lt F, Rt P	Lt Fr	M-hypo	n.d.	VPA, PHT, PB, CBZ, PRM, ZNS, CZP
6	M	28	LRE	CPS	Weekly	Rt P, Rt O	Lt O	Rt P	n.d.	VPA, PHT, CBZ
7	M	24	LRE	CPS	Daily	Rt Fr[a]	Rt Fr	M-hypo	Rt Fr[b]	VPA, PHT, CBZ, ZNS, CLB
8	M	4	WS→LRE	CPS	Monthly	Lt Fr, Lt P[a], Rt T, Rt P	Rt Fr, Rt T, Rt P, Rt O	None	n.d.	CZP, ZNS, VPA, PHT, CBZ, CLB
9	F	13	LRE	CPS	Monthly	Lt Fr, Lt P	Lt P, Rt O	M-hypo	n.d.	VPA, ZNS, CBZ, CZP
10	F	15	LRE	CPS	Daily	Lt Fr, Rt Fr, Rt P	Lt Fr, Rt Fr, Rt P	Rt Fr,T,Lt T	n.d.	PB, VPA, CBZ, PHT, ACZ, ESM, ZNS, SLT, NZP
11	M	21	WS→LRE	CPS	Weekly	Rt Fr, Rt O	Lt O, Rt Fr	M-hypo	n.d.	DZP, VPA, NZP, PB, CLB, PRM, CZP, CBZ, PHT
12	F	40	LRE	CPS	Weekly	Lt Fr, Lt P, Rt Fr, Rt P	Rt P, Rt T	Bil Fr,P, Rt O,P	n.d.	CZP, PHT, PB, CLB
13	F	2	WS→LRE	CPS	Monthly	Lt Fr, Rt Fr, Rt T, Rt P	None	Bil Fr,P	n.d.	NZP, CBZ, VPA, ZNS, PHT, CLB, CBZ, KBr
14	F	16	LRE	CPS	Daily	Rt Fr, Rt P	None	None	n.d.	VPA, ESM, ZNS, CZP, PHT, CBZ, APT
15	F	13	LRE	CPS	Monthly	Lt Fr, Lt T, Rt F	None	Rt Fr	n.d.	CBZ, ZNS, CZP, CLB
	Mean,	16.3								

F, female; M, male; WS, West syndrome; LRE, localization-related epilepsy; CPS, complex partial seizure; sGTC, secondarily generalized tonic–clonic convulsion; Lt, left; Rt, right; Bil, bilateral; Fr, frontal; P, parietal; T, temporal; O, occipital; M-hypo, multiple hypoperfusion areas; n.d., not done; None, no detectable findings; AED, antiepileptic drug; APT, acetylpheneturide; ACZ, acetazolamide; CBZ, carbamazepine; CLB, clobazam; CZP, clonazepam; DZP, diazepam; ESM, ethosuximide; KBr, potassium bromide; NZP, nitrazepam; PB, phenobarbital; PHT, phenytoin; PRM, primidone; SLT, sulthiame; VPA, valproate acid; ZNS, zonisamide.

[a]Calcified tuber.

[b]Findings on 3D-SSP and SISCOM.

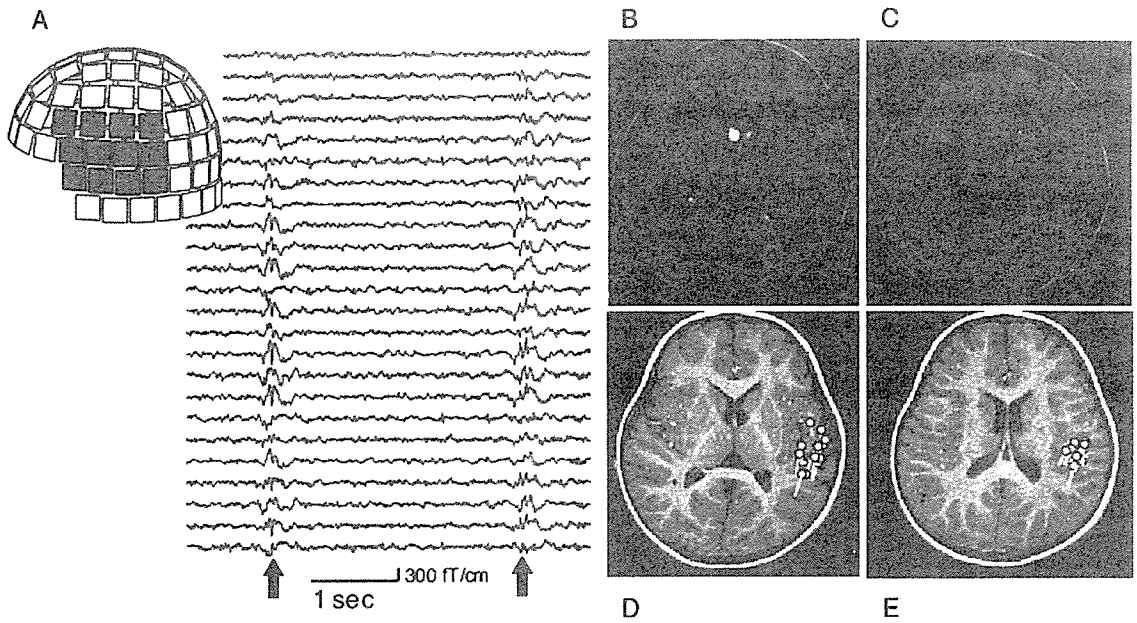

FIG. 1. Raw interictal magnetoencephalography (MEG) data recorded from 24 sensors covering the left temporal area, fluid-attenuated inversion recovery (FLAIR) magnetic resonance imaging (MRI) and an equivalent current dipole (ECD) cluster from spike discharges on MEG: Case 1. **A:** Raw interictal MEG data: MEG spikes were clearly identified from sensors covering the left temporal area (*arrows*). **B, C:** FLAIR MRI shows multiple high-intensity areas. **D, E:** An ECD cluster from spike discharges on MEG (white) are superimposed on T_1-weighted MRI. ECDs are located adjacent to and surrounding the cortical tubers in the left frontal and temporal lobes.

RESULTS

Table 1 summarizes the clinical data and results of investigations.

MRI

PDW and FLAIR MRI clearly demonstrated cortical tubers as hyperintense areas in all TS patients (Figs. 1B and C, 2A, and 3A). On the whole, cortical tubers were diffusely disseminated throughout the cerebral cortices or around the lateral ventricles. In 11 of 15 patients (cases 1–4, 8–14), multiple (more than five) cortical tubers were detected. The remaining patients (cases 5–7, 15) had two or three tubers.

MEG

In six (40.0%) of 15 patients (cases 1–5, 7), ECDs were clustered in the area adjacent to and surrounding one specific cortical tuber, suggesting that this was the epileptic focus (Figs. 1 A, D, and E, 2B, and 3B). In five (33.3%) of 15 patients (cases 8–12), ECDs were localized to areas surrounding two or three independent cortical tubers. In one (6.7%) patient, ECDs were clustered in an area where no definite cortical tuber was seen on PDW and FLAIR MRI (case 6). In three (20%) of 15 patients, no ECD clusters were detected (cases 13–15). Other than the fact that ECDs were generally located around tubers, the orientations of ECD clusters were random.

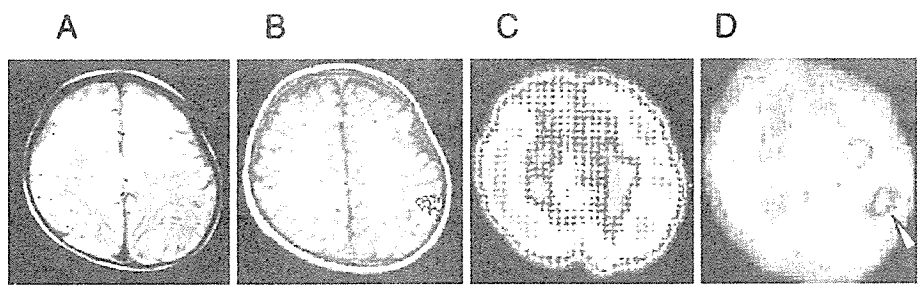

FIG. 2. Magnetic resonance imaging (MRI), magnetoencephalography (MEG), and single-photon emission computed tomography (SPECT) findings: Case 2. **A:** Proton density-weighted MRI reveals diffuse multiple high-intensity areas, indicating cortical tubers. **B:** MEG: An equivalent current dipole (ECD) cluster (yellow), superimposed on T_1-weighted MRI, is detected in the left parietal lobe. **C:** Interictal SPECT: Hypoperfusion areas are shown in the right frontal and the left parietal lobes. **D:** Ictal SPECT: A hyperperfusion area (*white arrowhead*) is seen in the left parietal area. It is spatially consistent with an ECD cluster on MEG. Another hyperperfusion area is regarded as secondary hyperperfusion because of cortical tubers.

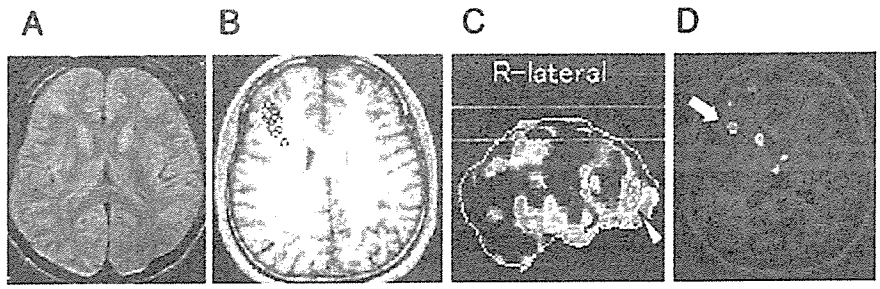

FIG. 3. Magnetic resonance imaging (MRI), magnetoencephalography (MEG), and single-photon emission computed tomography (SPECT) findings: Case 7. **A:** Proton density-weighted MRI: High-intensity areas are seen in the right frontotemporal and the left frontal lobes. **B:** MEG: An equivalent current dipole (ECD) cluster (yellow) is detected adjacent to and surrounding a single tuber in the right frontal lobe. **C, D:** Ictal SPECT: On simple ictal SPECT, no hyperperfusion area is recognized (data not shown). However, after processing of original images by using 3D-SSP **(C)** or SISCOM **(D)** technology, a hyperperfusion area, indicated by a *white arrowhead* **(C)** and a *white arrow* **(D)**, emerged in the right frontal lobe. These images are spatially consistent with the location of an ECD cluster on MEG.

SPECT

In interictal SPECT, multiple hypoperfusion areas consistent with cortical tubers on MRI were apparent in 10 (66.7%) of 15 patients (cases 2–5, 7, 9–13) (Fig. 2C). A single hypoperfusion area was detected in two (13.3%) patients (cases 6 and 15). No hypoperfusion areas were found in three (20.0%) patients (cases 1, 8, and 14).

Although interictal abnormal SPECT findings were not consistent with MEG spike foci in all 15 patients, ictal SPECT obtained from cases 2 and 7 showed hyperperfusion areas consistent with MEG spike foci (Figs. 2D, and 3C and D).

Surgery

After preoperative evaluation, surgery was performed in three patients (cases 2, 4, and 7), all of whom exhibited a single ECD cluster on MEG. In case 2, localization of ECDs was consistent with the hyperperfusion area on ictal SPECT, and this region was resected. Although seizures recurred immediately after the operation, appropriate AEDs eventually eliminated seizures. In case 4, although ictal SPECT was unsuccessful, MEG findings were spatially consistent with the onset zone of seizures on ictal electrocorticography (ECoG). Seizures disappeared postoperatively in this case. Patient 7 underwent surgical resection according to the findings of MEG, ECoG, SISCOM, and 3D-SSP. No seizures have occurred postoperatively. Over a mean follow-up period of 36 months, cases 4 and 7 were assessed as seizure free, and case 2 also achieved >90% seizure reduction. Postoperative MEG showed no residual spike discharge in cases 4 and 7; however, residual ECDs were confirmed around the resected region in case 2. After surgery, higher brain functions were measured by WAIS-R (case 7) or Suzuki-Binet (case 4) in cases 4 and 7 when compared with that measured preoperatively. Patient 2 was too young to undergo evaluation of cognitive function. However, in this patient, development progressed gradually, and surgical intervention prevented deterioration: his developmental quotient remained very similar preoperatively and 3 years postoperatively. In all three patients, AEDs requirements were reduced postoperatively.

DISCUSSION

We investigated the localization of ECDs on MEG in 15 patients with concurrent TS and LRE. Of 15 patients, six (40.0%) exhibited a single ECD cluster around a single tuber, whereas five (33.3%) demonstrated ECDs around two or more tubers. On MRI, 11 patients showed multiple (more than five) cortical tubers, and the remaining patients had two or three tubers, confirming the findings observed in previous reports of TS (14). Although multiple tubers were present, ECDs were detected only adjacent to and surrounding epileptogenic tubers. The present MEG findings implied that a single epileptic focus might have been present in several of the TS patients, even though multiple tubers were observed on MRI. In three cases in our series, localized ECDs were not detected. Previously, only two authors described MEG findings in small numbers of TS patients evaluated with limited sensor arrays (9,10). We reported MEG findings in TS for a large number of patients evaluated with whole-head MEG systems. As TS is characterized by multiple lesions throughout the brain, we consider a whole-head MEG system to be appropriate for evaluating such patients. With such an apparatus, we successfully revealed ECDs located adjacent to and surrounding specific tubers among multiple brain lesions in TS. ECDs were located in an area where no cortical tubers were observed on PDW and FLAIR MRI in only one patient. MRI is not yet sophisticated enough to depict all the cortical tubers that can be identified by gross inspection of the sectioned brain (15,16). Moreover, the correlation between MRI and EEG findings is not absolute (16). It is accordingly possible that latent cortical tubers that are not detected by MRI may have strong epileptogenic activity.

Surgical indications and procedures for patients with TS and epileptic seizures are still controversial. Some authors stress the difficulty of surgical treatments for TS patients with multiple tubers and LRE (17). No crucial

criteria exist for selecting surgical candidates in this patient group. We performed both focus resection and tuberectomy in three patients with a single ECD cluster on MEG and found MEG findings to be useful in determining the specific tuber directly related to the epileptic focus. In the present series, two patients achieved a seizure-free outcome, whereas seizure frequency decreased and AEDs could be reduced in another. Postoperative MEG indicated that all epileptogenic regions had been resected in two patients; however, residual seizures might relate to the residual ECDs around the resected region in case 2. Our findings strongly suggest that ECD clusters are well correlated with epileptogenic zones and that TS patients with medically refractory LRE who exhibit a single ECD cluster on MEG may be appropriate candidates for surgical treatment. However, isolated lesionectomy based on MRI findings alone might be insufficient to control future seizure foci (18).

Focal cortical dysplasia (FCD) is an organic lesion characterized by an epileptogenic cerebral cortical nodule. Several authors have reported MEG findings for patients with FCD, indicating that ECDs of spike discharges were located in the actual FCD nodules (19–21). However, in 11 of our series of 15, ECDs were located in the vicinity of tuberous nodules, a finding in accordance with previous reports (9,10). A recent study using molecular biologic techniques described the relation between FCD of Taylor's balloon cell type and mutation of the *TSC1* gene (22). FCD is well known to have intrinsic epileptogenicity. Our results, however, suggest that the epileptic focus in TS is not anticipated to be within lesions visible on MRI, as is the case in dysembryoplastic neuroepithelial tumor (23). Hence it cannot be assumed that tuberectomy is an ideal surgical strategy for epilepsy patients with TS.

On interictal SPECT, most tubers were recognized as hypoperfusion areas. In SLRE, epileptogenic areas often demonstrate hyperperfusion in the ictal phase and hypoperfusion in the interictal period (24,25). It is difficult to identify epileptogenic areas by interictal SPECT in TS, as multiple tubers give rise to many hypoperfusion areas. We therefore consider MEG to be far superior to interictal SPECT in identifying true epileptic foci in patients with TS. Conversely, Koh (6) reported that ictal SPECT revealed hyperperfusion areas corresponding to epileptogenic lesions in 10 of 21 patients with TS and LRE. We also confirmed ictal hyperperfusion areas consistent with localization of ECDs on MEG in two cases. Although ictal SPECT findings are considered reliable in determining epileptogenic regions, unfortunately epileptic seizures are usually unpredictable. It is therefore not feasible to perform ictal SPECT in every case. Our findings indicate that despite the recording of interictal phenomena, MEG is as useful as ictal SPECT for identifying epileptic foci in patients with TS.

In conclusion, whole-head MEG revealed ECD clusters adjacent to and surrounding epileptogenic tubers. This suggests that epileptic foci are located in the extrinsic area surrounding the tubers. Hence our study provides support for the role of MEG in enabling precise identification of true epileptic foci and providing crucial information for surgical planning in patients with TS and intractable epilepsy. It should be emphasized that TS patients with a single ECD cluster on MEG may be appropriate candidates for surgical treatment. The present study also suggests that interictal MEG could be substituted for ictal SPECT in epilepsy patients with TS; however, analysis of further similar cases is needed to confirm this.

Acknowledgment: We thank Ms. Kuniko Tsuchiya for excellent technical assistance. This study was supported in part by the Research Grant (17A-11) for Nervous and Mental Disorders from the Ministry of Health, Labour, and Welfare.

REFERENCES

1. Kotagal P. Epilepsy in the setting of neurocutaneous syndromes. In: Wyllie E, ed. *The Treatment of Epilepsy: Principles and Practice*. 3rd ed. Philadelphia: Lippincott Williams & Wilkins, 2001:627–636.
2. Rintahaka PJ, Chugani HT. Clinical role of positron emission tomography in children with tuberous sclerosis complex. *J Child Neurol* 1997;12:42–52.
3. Cheadle JP, Reeve MP, Sampson JR, et al. Molecular genetic advances in tuberous sclerosis. *Hum Genet* 2000;107:97–114
4. Chiron C, Dumas C, Jambaqué I, et al. Randomized trial comparing vigabatrin and hydrocortisone in infantile spasms due to tuberous sclerosis. *Epilepsy Res* 1997;26:389–395.
5. Bebin EM, Kelly PJ, Gomez MR. Surgical treatment for epilepsy in cerebral tuberous sclerosis. *Epilepsia* 1993;34:651–657.
6. Koh S, Jayakar P, Resnick T, et al. The localizing value of ictal SPECT in children with tuberous sclerosis complex and refractory partial epilepsy. *Epileptic Disord* 1999;1:41–46.
7. Avellino AM, Berger MS, Rostomily RC, et al. Surgical management and seizure outcome in patients with tuberous sclerosis. *J Neurosurg* 1997;87:391–396.
8. Guerreiro MM, Andermann F, Andermann E, et al. Surgical treatment of epilepsy in tuberous sclerosis: strategies and results in 18 patients. *Neurology* 1998;51:1263–1269.
9. Peresson M, Lopez L, Narici L, et al. Magnetic source imaging and reactivity to rhythmical stimulation in tuberous sclerosis. *Brain Dev* 1998;20: 512–518.
10. Kubota M, Ichiseki H, Takeshita K, et al. Magnetoencephalographic study of epileptic foci in patients with tuberous sclerosis. In: Yoshimoto T, Kotani M, Kuriki Set al., eds. *Recent Advances in Biomagnetism*. Sendai: Tohoku University Press, 1999:774–777.
11. Commission on Classification and Terminology of the International League Against Epilepsy. Proposal for revised classification of epilepsies and epileptic syndromes. *Epilepsia* 1989;30:389–399.
12. Minoshima S, Frey KA, Koeppe RA, et al. A diagnostic approach in Alzheimer's disease using three-dimensional stereotactic surface projections of Fluorine-18-FDG PET. *J Nucl Med* 1995;36:1238–1248.
13. O'Brien TJ, So EL, Mullan BP, et al. Subtraction ictal SPECT co-registered to MRI improves clinical usefulness of SPECT in localizing the surgical seizure focus. *Neurology* 1998;50:445–454.
14. Barkovich AJ. *Pediatric Neuroimaging*. 3rd ed. Philadelphia: Lippincott Williams & Wilkins, 2000.
15. Nixon JR, Miller GM, Okazaki H, et al. Cerebral tuberous sclerosis: postmortem magnetic resonance imaging and pathologic anatomy. *Mayo Clin Proc* 1989;64:305–311.

16. Curatolo P. Tuberous sclerosis: relationships between clinical and EEG findings and magnetic resonance imaging. In: Guerrini R, Andermann F, Canapicchi Ret al., eds. *Dysplasias of Cerebral Cortex and Epilepsy*. Philadelphia: Lippincott-Raven, 1996:191–198.
17. Romanelli P, Najjar S, Weiner HL, et al. Epilepsy surgery in tuberous sclerosis: multistage procedures with bilateral or multilobar foci. *J Child Neurol* 2002;17:689–692.
18. Curatolo P, Bombardieri R, Verdecchia M, et al. Intractable seizures in tuberous sclerosis complex: from molecular pathogenesis to the rationale for treatment. *J Child Neurol* 2005;20:318–325.
19. Morioka T, Nishio S, Ishibashi H, et al. Intrinsic epileptogenicity of focal cortical dysplasia as revealed by magnetoencephalography and electrocorticography. *Epilepsy Res* 1999;33:177–187.
20. Hader WJ, Mackay M, Otsubo H, et al. Cortical dysplastic lesions in children with intractable epilepsy: role of complete resection. *J Neurosurg Pediatr* 2004;100:110–117.
21. Bast T, Oezkan O, Rona S, et al. EEG and MEG source analysis of single and averaged interictal spikes reveals intrinsic epileptogenicity in focal cortical dysplasia. *Epilepsia* 2004;45:621–631.
22. Becker AJ, Urbach H, Scheffler B, et al. Focal cortical dysplasia of Taylor's balloon cell type: mutational analysis of the *TSC1* gene indicates a pathogenic relationship to tuberous sclerosis. *Ann Neurol* 2002;52:29–37.
23. Kameyama S, Fukuda M, Tomikawa M, et al. Surgical strategy and outcomes for epileptic patients with focal cortical dysplasia or dysembryoplastic neuroepithelial tumor. *Epilepsia* 2001;42(suppl 6):37–41
24. Bonte FJ, Devous MD Sr, Stokely EM, et al. Single-photon tomographic determination of regional cerebral blood flow in epilepsy. *AJNR Am J Neuroradiol* 1983;4:544–546.
25. Stefan H, Schneider S, Feistel H, et al. Ictal and interictal activity in partial epilepsy recorded with multichannel magnetoelectroencephalography: correlation of electroencephalography/electrocorticography, magnetic resonance imaging, single photon emission computed tomography, and positron emission tomography findings. *Epilepsia* 1992;33:874–887.

Cholesterol depletion facilitates ubiquitylation of NPC1 and its association with SKD1/Vps4

Yuki Ohsaki[1], Yuko Sugimoto[1], Michitaka Suzuki[1], Hiroshi Hosokawa[2], Tamotsu Yoshimori[3], Joanna P. Davies[4], Yiannis A. Ioannou[4], Marie T. Vanier[5], Kousaku Ohno[6] and Haruaki Ninomiya[1,*]

[1]Department of Neurobiology, Tottori University Faculty of Medicine, Yonago 683-8503, Japan
[2]Department of Intelligence Science and Technology, Graduate School of Informatics, Kyoto University, Kyoto 606-8501, Japan
[3]Department of Cell Genetics, National Institute of Genetics, Mishima 411-8540, Japan
[4]Department of Human Genetics, Mount Sinai School of Medicine, New York, NY 10029, USA
[5]INSERM Unit 189, Lyon-Sud Medical School and Fondation Gillet-Merieux, Lyon-Sud Hospital, 69921 Oullins, France
[6]Department of Child Neurology, Tottori University Faculty of Medicine, Yonago 683-8503, Japan
*Author for correspondence (e-mail: ninomiya@grape.med.tottori-u.ac.jp)

Accepted 23 March 2006
Journal of Cell Science 119, 2643-2653 Published by The Company of Biologists 2006
doi:10.1242/jcs.02993

Summary

Niemann-Pick disease type C (NPC) is an inherited lipid storage disorder caused by mutations in *NPC1* or *NPC2*. NPC1 is a polytopic glycoprotein that contains a sterol-sensing domain, whereas NPC2 is a soluble protein that contains an MD-2-like lipid-recognition domain. In the current study, we addressed the hypothesis that ubiquitylation of NPC1 might be regulated by cholesterol. We found that depletion of cellular cholesterol facilitated ubiquitylation of NPC1 expressed in COS cells. A loss-of-function mutant, NPC1(P691S), which contains an amino acid substitution in the sterol-sensing domain, failed to respond to cholesterol depletion. Another mutant, NPC1(δLLNF), which lacks the endosomal-targeting motif, also failed to respond. SKD1(E235Q), a dominant-negative mutant of SKD1/Vps4 that inhibits disassembly of the endosomal sorting complex required for transport (ESCRT), caused an accumulation of ubiquitylated NPC1. SKD1(E235Q) associated with NPC1 on the endosomal membrane, whereas wild-type SKD1 associated with NPC1 only when cells were depleted of cholesterol. Similarly, in control human skin fibroblasts, cholesterol depletion facilitated ubiquitylation of endogenous NPC1. In patient cells that lack NPC2 function, NPC1 was ubiquitylated regardless of cellular cholesterol levels, suggesting that NPC2 is required to prevent NPC1 ubiquitylation under cholesterol-rich conditions. These results suggest that ubiquitylation of NPC1 and its association with the ESCRT complex are controlled by endosomal cholesterol levels utilizing a mechanism that involves NPC2.

Key words: NPC1, NPC2, SKD1, Vps4, Ubiquitin, Cholesterol

Introduction

Niemann-Pick disease type C (NPC) is an autosomal recessive lipid storage disorder that is characterized by endosomal accumulation of low-density lipoprotein (LDL)-derived cholesterol (Patterson et al., 2001) and is caused by mutations in *NPC1* or *NPC2* (Carstea et al., 1997; Naureckiene et al., 2000). NPC1 is a membrane protein that resides primarily in the late endosome (Higgins et al., 1999), whereas NPC2 is a soluble protein that resides primarily in the lysosome (Vanier and Millat, 2004). These two proteins have been shown to function in the same endosomal cholesterol efflux pathway (Sleat et al., 2004). However, it is not clear how they interact with each other.

Solution of the human NPC1 membrane topology revealed a 1278 amino acid protein with 13 transmembrane domains and a sterol-sensing domain (SSD) located from transmembrane domains III to VII (Davies and Ioannou, 2000). Although this protein has been shown to possess a lipid permease activity (Davies et al., 2000) and the functional significance of its SSD has been well documented (Watari et al., 1999a; Millard et al., 2005), it is not known whether NPC1 function is regulated by cellular cholesterol. In addition to NPC1, SSDs are found in other proteins involved in the control of cellular cholesterol homeostasis: sterol regulatory element binding protein (SREBP) cleavage-activating protein (SCAP) and 3-hydroxy-3-methylglutaryl CoA reductase (HMG-CoAR), both of which reside primarily in the endoplasmic reticulum (ER). SCAP associates with the ER-retention proteins, Insig-1 and Insig-2, in a sterol-dependent manner: when cells are depleted of cholesterol, SCAP, together with SREBP, is released from the Insig proteins and transported to the Golgi apparatus, where a mature, active form of SREBP is generated by proteolysis and stimulates transcription of a diverse set of genes involved in cholesterol uptake and synthesis (Yang et al., 2002; Yabe et al., 2002). Similarly, HMG-CoAR associates with the Insig proteins in a sterol-dependent manner, but in this case, the association facilitates its ubiquitylation and subsequent degradation by the proteasome, thus shutting off endogenous cholesterol biosynthesis (Ravid et al., 2000; Sever et al., 2003a; Sever et al., 2003b). By analogy, one might hypothesize a cholesterol-dependent regulation of NPC1 function, either by its association with other proteins or by post-translational modifications.

Yeast genetic analysis has identified a number of proteins required for trafficking of endosomal proteins to the vacuole,

collectively termed the vacuolar protein sorting (Vps) proteins. These proteins assemble on the endosomal membrane to form the protein complexes ESCRT (endosomal sorting complex required for transport) -I, -II and -III, which operate sequentially (Katzmann et al., 2001; Babst et al., 2002a; Babst et al., 2002b). In this sorting process, ubiquitylation of an endosomal membrane protein serves as a signal for its sorting into the internal membranes of multivesicular bodies (Hicke, 2001). Vps4 is an ATPase that exists primarily in an inactive, ADP-bound cytosolic form and its active, ATP-bound form can transiently associate with the endosomal membrane. This protein is required for disassembly of the ESCRT-III. Expression of an ATPase-deficient, dominant-negative mutant of Vps4, the E233Q mutant, results in entrapment of ubiquitylated proteins on the endosomal membrane (Babst et al., 1997; Babst et al., 1998). Ncr1 is the yeast homolog of NPC1 and recent studies provided two lines of evidence that indicated a functional interaction between Ncr1 and Vps4. First, the targeting of Ncr1 to the vacuolar limiting membrane depends on Vps proteins, including Vps4 (Zhang et al., 2004). Second, Ncr1-null and Vps4-null cells share the same phenotype – resistance to the ether lipid drug edelfosine (Berger et al., 2005).

Mammalian counterparts to Vps proteins are presumed to function in a similar manner, and have been shown to be required for the ubiquitin-dependent, lysosomal transport of various membrane proteins, such as epidermal growth factor receptor (EGFR) (Bishop and Woodman, 2000; Bishop et al., 2002), G-protein-coupled receptors (Shenoy et al., 2001) and the cystic fibrosis transmembrane conductance regulator (Sharma et al., 2004). The suppressor of potassium transport growth defect protein 1, SKD1, is a mammalian ortholog of Vps4 and is a member of the *N*-ethylmaleimide-sensitive factor and AAA-type ATPase family (Scheuring et al., 2001). Like Vps4 in yeasts, SKD1 shuttles between an ADP-bound cytosolic form and an ATP-bound membrane-associated form. Also, similar to Vps(E233Q), SKD1(E235Q) lacks the ATPase activity and has a dominant-negative effect when expressed in mammalian cells. Expressed SKD1(E235Q) protein disrupts endosomal trafficking and localizes to aberrant endosomes (Yoshimori et al., 2000; Fujita et al., 2003).

Given the presence of an SSD, we hypothesized that NPC1 might be ubiquitylated by a cholesterol-dependent mechanism. Following confirmation that cellular cholesterol depletion facilitated NPC1 ubiquitylation, we pursued the hypothesis further that NPC1 interacts with the ESCRT complex.

Results

Cholesterol depletion facilitated ubiquitylation of NPC1 expressed in COS cells

NPC1 ubiquitylation was examined in COS cells transfected with Flag-NPC1 and myc/His_6-ubiquitin. 48 hours after transfection, cells were incubated either in cholesterol-rich medium [DMEM + 10% bovine calf serum (BCS)] or cholesterol-depleted medium [DMEM + 10% lipoprotein-deficient serum (LPDS)] supplemented with compactin and mevalonate. When cells were incubated in the cholesterol-depleted medium, the total cellular cholesterol level decreased in a time-dependent manner to reach ~60% of the control level at 12 hours. The cholesterol level was restored by supplementation with 20 μg/ml LDL (Fig. 1A). Expressed Flag-NPC1 was recovered by immunoprecipitation with anti-Flag M2 agarose and the products were analyzed by immunoblotting. As expected, Flag-NPC1 was detected in the immunoprecipitation products as a broad band between 150 and 250 kDa, as a result of its extensive glycosylation (Watari et al., 1999a). In addition, a band just below the top of the gel was often observed (for example, see Fig. 1E), which might represent an oligomerized form of the protein. Cholesterol depletion had little, if any, effect on the steady-state levels of the expressed proteins. However, probing with anti-myc revealed that cholesterol depletion caused conjugation of myc/His_6-ubiquitin to Flag-NPC1 (Fig. 1B). The positive signals were constantly detected at 6 hours and were sustained up to 24 hours. The conjugation was also demonstrated by metal affinity purification of myc/His_6-ubiquitin. Flag-NPC1 was detectable in the affinity purification products from cholesterol-depleted cells (Fig. 1C, left panel). Probing the affinity purification products with anti-myc showed no overall increase of ubiquitylated proteins in cholesterol-depleted cells (Fig. 1C, right panel). To see whether the ubiquitylation was caused by overexpression of ubiquitin molecules, cells were transfected only with Flag-NPC1 construct. Probing the anti-Flag immunoprecipitation products with anti-ubiquitin P4D1 revealed conjugation of endogenous ubiquitin to Flag-NPC1 in cells depleted of cholesterol (Fig. 1D).

Next, by using myc/His_6-ubiquitin co-expression, we examined whether cholesterol, instead of LDL, could suppress Flag-NPC1 ubiquitylation. Supplementation of the cholesterol-depleted medium with free cholesterol caused dose-dependent suppression of Flag-NPC1 ubiquitylation (Fig. 1E), suggesting that the ubiquitylation was a result primarily to cholesterol depletion.

To characterize Flag-NPC1 ubiquitylation further, we conducted two lines of experiments, first to examine effects of U18666A and second to examine detergent solubility of ubiquitylated Flag-NPC1. U18666A is a sterol derivative that has been shown to induce an NPC-like phenotype (Ko et al., 2001). To see whether this compound affected Flag-NPC1 ubiquitylation, transfected cells were incubated with 2 μg/ml U18666A for 12 hours. U18666A treatment at this concentration and duration caused endosomal cholesterol accumulation as revealed by filipin staining (data not shown) and, as reported previously (Sugimoto et al., 2001), an increase in the steady-state levels of expressed Flag-NPC1. Despite its effects on the steady-state levels, U18666A did not affect Flag-NPC1 ubiquitylation in cholesterol-rich medium nor did it suppress Flag-NPC1 ubiquitylation in cholesterol-depleted medium (Fig. 1F).

Cholesterol is the major constituent of raft microdomains and a part of NPC1 has been shown to associate with these domains (Garver et al., 2000). Therefore, it was possible that cholesterol depletion changed distribution of Flag-NPC1, which might lead to its ubiquitylation. To test this possibility, we examined the levels of Flag-NPC1 and its ubiquitylated form in 1% Triton X-100-soluble and Triton X-100-insoluble fractions, since raft microdomains are preferentially recovered in the insoluble fractions (Simons and Ikonen, 1997). Incubation for 6 hours in the cholesterol-depleted medium

reduced the level of Flag-NPC1 recovered from insoluble fractions. However, ubiquitylated Flag-NPC1 was recovered both from soluble and insoluble fractions (Fig. 1G). These data did not support the notion that Flag-NPC1 ubiquitylation was secondary to re-distribution of the protein between raft and non-raft membrane domains.

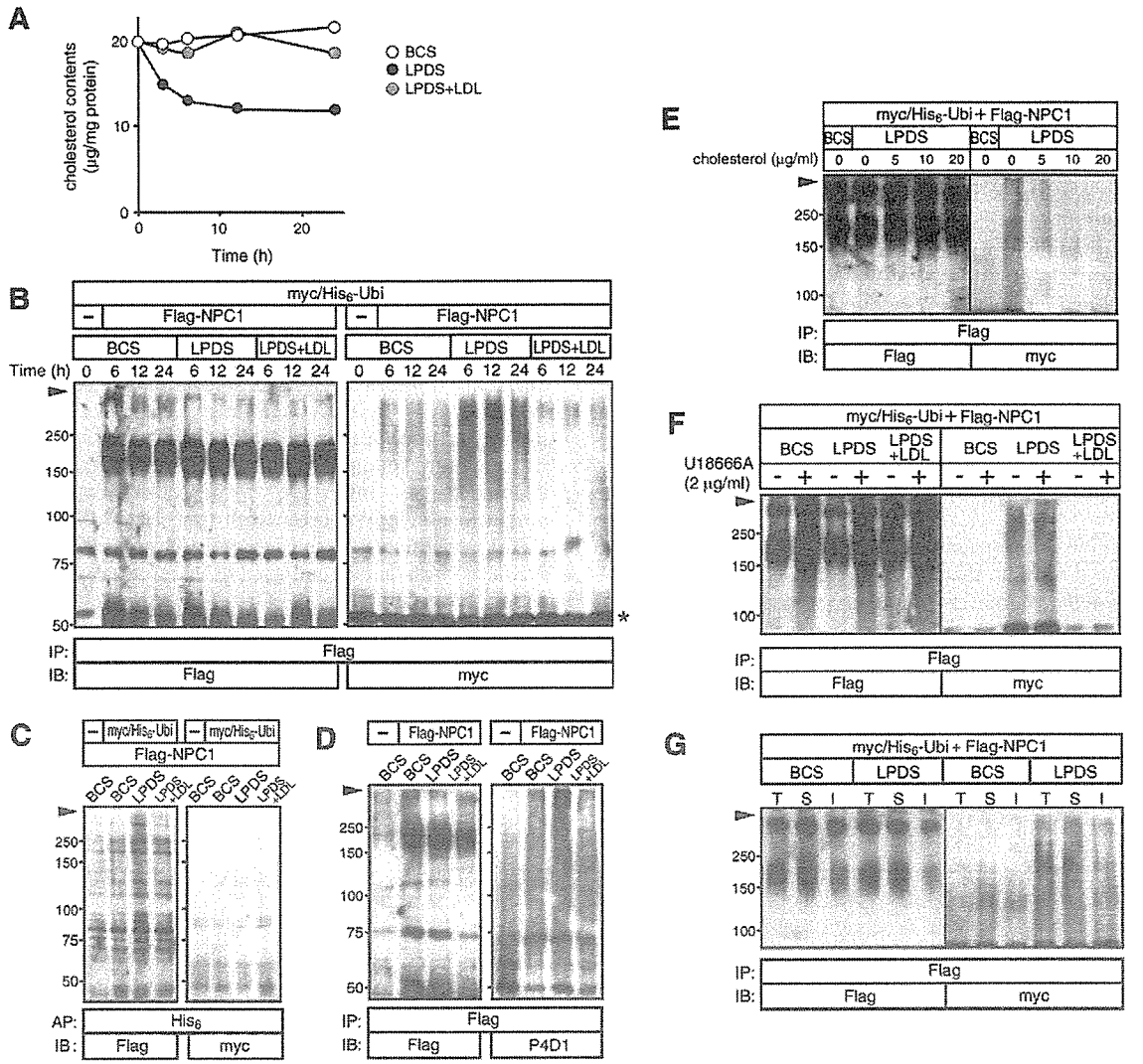

Fig. 1. Effects of cholesterol depletion on ubiquitylation of Flag-NPC1 expressed in COS cells. (A) Cellular cholesterol levels. Cells were cultured in cholesterol-rich medium (DMEM + 10% BCS) or cholesterol-depleted medium (DMEM + 10% LPDS supplemented with compactin and mevalonate) with or without LDL (20 μg/ml) up to 24 hours. Concentrations of total cholesterol in cell lysates were determined as described in the Materials and Methods. Each point represents the mean of duplicated determinations obtained in a single experiment. (B) Conjugation of myc/His_6-ubiquitin (myc/His_6-Ubi) to Flag-NPC1. Cells were transfected with expression constructs for myc/His_6-ubiquitin together with Flag-NPC1 or an empty vector. 48 hours after transfection, they were further cultured in the indicated medium. 0.5% CHAPS extracts were subjected to anti-Flag immunoprecipitation (IP) followed by immunoblotting (IB) with indicated antibodies. Molecular weights are given on the left (kDa). The arrowhead indicates the top of the separating gel and the asterisk indicates the heavy chain. (C) Co-purification of Flag-NPC1 with myc/His_6-ubiquitin. After incubation in the indicated medium for 6 hours, cell extracts were subjected to affinity purification with metal resin followed by immunoblotting with indicated antibodies. (D) Conjugation of endogenous ubiquitin to Flag-NPC1. Cells were transfected with Flag-NPC1 or an empty vector, cultured in the indicated medium for 6 hours and anti-Flag IP products were analyzed by indicated antibodies. (E) Effects of exogenous cholesterol on ubiquitylation of Flag-NPC1. Cells were transfected with myc/His_6-ubiquitin and Flag-NPC1, and cultured for 6 hours in cholesterol-rich or cholesterol-depleted medium supplemented with increasing concentrations of cholesterol. (F) Effects of U18666A. The transfected cells were cultured in the indicated medium for 12 hours in the presence or absence of U18666A. (G) Solubility of Flag-NPC1 to 1% Triton X-100. The transfected cells were cultured in the indicated medium for 6 hours. Total cell extracts (T), 1% Triton X-100-soluble (S) and Triton X-100-insoluble (I) fractions were prepared as described in the Materials and Methods. In E-G, anti-Flag immunoprecipitation products were subjected to immunoblotting with anti-Flag or anti-myc. All results shown are representative and were reproduced at least twice.

Mutant proteins Flag-NPC1(P691S) and Flag-NPC1(δLLNF) failed to respond to cholesterol depletion

To examine the role of the SSD in the cholesterol-level-dependent ubiquitylation, myc/His_6-ubiquitin co-expression experiments were repeated using Flag-NPC1(P691S), a loss-of-function mutant that contains an amino acid substitution in its SSD (Watari et al., 1999a; Millard et al., 2005). Anti-Flag immunoprecipitation products contained similar levels of Flag-NPC1 wild-type (wt) and P691S mutant proteins. Probing with anti-myc demonstrated that, in contrast to the wt protein, ubiquitylation of this mutant protein was barely facilitated following cholesterol depletion for 6 hours (Fig. 2A). To examine whether endosomal localization was required for NPC1 to undergo this modification, we examined effects of cholesterol depletion on the δLLNF mutant protein that lacks the C-terminal di-leucine motif and is retained in the ER (Watari et al., 1999b; Scott et al., 2004). As in the case of the P691S mutant, ubiquitylation of this mutant protein was barely affected by cholesterol depletion (Fig. 2B).

As a control experiment, we examined the effects of MG132, a proteasome inhibitor, on ubiquitylation of expressed proteins and found similar responses of the wt and mutant proteins. Similar to the wt protein, both P691S and δLLNF mutant proteins were extensively ubiquitylated in cells treated with 5 μM MG132 for 6 hours (Fig. 2).

Effects of MG132 and leupeptin on ubiquitylation of NPC1

Ubiquitylation can serve as a signal for protein degradation, which is executed by the cytosolic proteasome or by the lysosome. In an attempt to see whether ubiquitylated NPC1 underwent proteasomal and/or lysosomal degradation, we compared effects of MG132 and the lysosomal inhibitor leupeptin on Flag-NPC1 ubiquitylation. Treatment with 5 μM MG132 for 6 hours caused accumulation of ubiquitylated Flag-NPC1 and its effects were not influenced by cellular cholesterol levels. This increase in ubiquitylated Flag-NPC1 was accompanied by increased steady-state levels of Flag-NPC1, again regardless of the cholesterol levels (Fig. 3, upper panel). Similar results were reproduced with the proteasome inhibitor lactocystin (10 μM) (data not shown). By contrast, treatment with 100 μM leupeptin for 6 hours did not affect ubiquitylation of Flag-NPC1 either in cholesterol-rich or cholesterol-depleted conditions, nor caused appreciable changes in the steady-state levels of the protein (Fig. 3, lower panel). Incubation of the cells with NH_4Cl (10 mM for 6 hours) also failed to affect ubiquitylation of Flag-NPC1 and its steady-state levels (data not shown).

Interaction between SKD1(E235Q) and NPC1

Ubiquitylation can serve as a signal for the intracellular sorting of a protein. Since NPC1 resides primarily in the late endosome, we hypothesized that NPC1 was recognized by the ESCRT complex, which plays an essential role in the lysosomal sorting of ubiquitylated endosomal proteins. To address this hypothesis, NPC1 ubiquitylation was examined in the presence of SKD1(E235Q) (Fig. 4A), which inhibits disassembly of the ESCRT complex. When transfected cells were cultured in cholesterol-rich medium, expression of His_6-SKD1wt did not affect ubiquitylation of Flag-NPC1, whereas expression of His_6-SKD1(E235Q) caused a clear increase in the level of ubiquitylated Flag-NPC1 (Fig. 4B). Given its

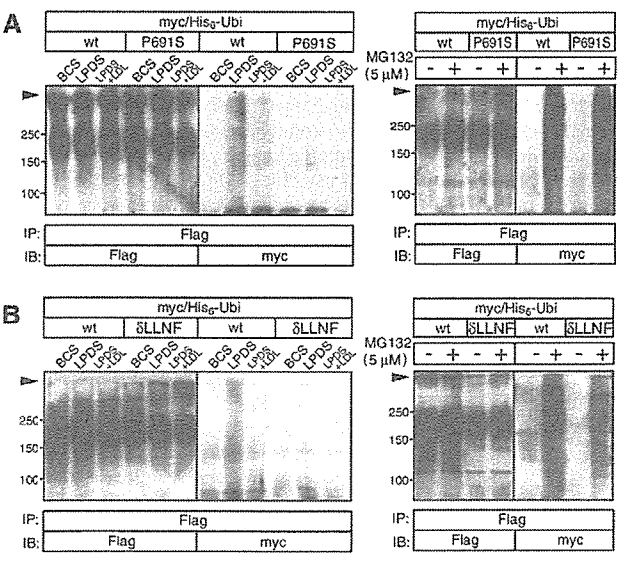

Fig. 2. Ubiquitylation of mutant NPC proteins. COS cells were transfected with myc/His_6-ubiquitin (myc/His_6-Ubi) together with Flag-NPC1 constructs that encoded the wild-type (wt) or mutant proteins P691S (A) or δLLNF (B); the arrowhead indicates the top of the separating gel. Cells were cultured in the indicated medium for 6 hours (left panels) or treated with or without MG132 for 6 hours (right panels). In both A and B, anti-Flag immunoprecipitation (IP) products were subjected to immunoblotting (IB) with anti-Flag or anti-myc. All results shown are representative and were reproduced at least twice.

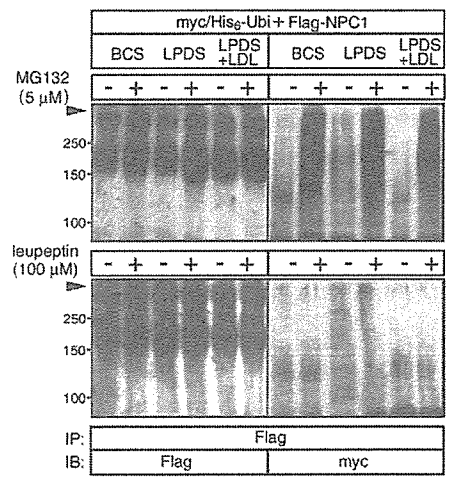

Fig. 3. Effects of MG132 and leupeptin on ubiquitylation of Flag-NPC1. COS cells were transfected with myc/His_6-ubiquitin (myc/His_6-Ubi) and Flag-NPC1 constructs, and were cultured in the indicated medium for 6 hours in the absence or presence of MG132 (upper panel) or leupeptin (lower panel); the arrowhead indicates the top of the separating gel. Anti-Flag immunoprecipitation (IP) products were subjected to immunoblotting (IB) with anti-Flag or anti-myc. All results shown are representative and were reproduced at least twice.

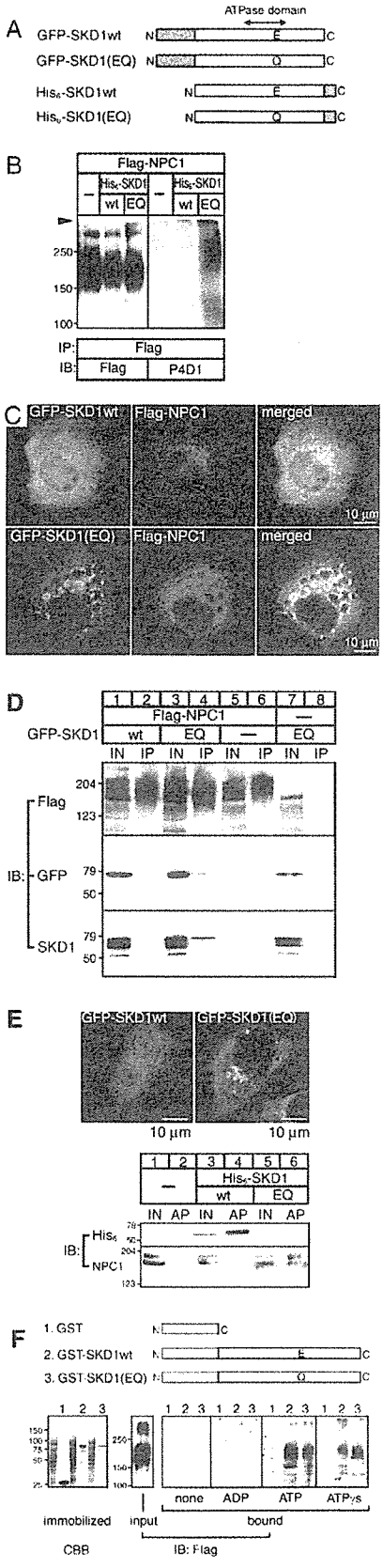

effects on NPC1 ubiquitylation, we examined whether SKD1(E235Q) co-localized and could interact with NPC1. Expression of a GFP-SKD1wt construct yielded a diffuse distribution in the cytoplasm and the nucleus, and did not induce any obvious changes of intracellular structures. Anti-Flag immunofluorescence revealed that Flag-NPC1 was retained in endosomes and did not co-localize with GFP-SKD1wt. As reported previously (Yoshimori et al., 2000; Fujita et al., 2003), expression of GFP-SKD1(E235Q) results in the formation of multiple aberrant vesicles that associated with the E235Q protein. Flag-NPC1 also localized to these aberrant endosomes and partially co-localized with GFP-SKD1(E235Q) (Fig. 4C). Detection of His_6-tagged SKD1 and Flag-NPC1 proteins yielded similar results (data not shown).

We next examined whether there was any interaction between Flag-NPC1 and SKD1 by immunoprecipitation and immunoblotting experiments. Similar levels of Flag-NPC1 were recovered by anti-Flag immunoprecipitation from cells expressing wt or E235Q mutant GFP-SKD1 protein (Fig. 4D, lanes 2 and 4). Probing the same immunoprecipitation products with anti-GFP showed that a portion of the GFP-SKD1(E235Q) protein was co-precipitated with Flag-NPC1

Fig. 4. Interaction between SKD1(E235Q) and NPC1. (A) Schematic representation of expressed SKD1 proteins. Each tag is shown in gray. (B) Flag-NPC1 ubiquitylation. COS cells were transfected with the Flag-NPC1 construct together with an empty vector or His_6-SKD1 constructs. 48 hours after transfection, anti-Flag immunoprecipitation (IP) products were subjected to immunoblotting (IB) with anti-Flag or anti-ubiquitin (P4D1). Molecular weights are given on the left (kDa); the arrowhead indicates the top of the separating gel. (C) Intracellular localization of GFP-SKD1 and Flag-NPC1. COS cells expressing Flag-NPC1 and GFP-SKD1 wild-type (wt; upper) or the E235Q mutant (EQ; lower) were fixed and stained with anti-Flag antibody. Bound antibody was visualized with Alexa Fluor 546-conjugated secondary antibody. Results shown are the representative images obtained with a confocal microscope. (D) Co-precipitation of Flag-NPC1 and GFP-SKD1 proteins. 0.5% CHAPS extracts were prepared from COS cells transfected with Flag-NPC1 together with GFP-SKD1wt or E235Q constructs. Anti-Flag immunoprecipitation products were analyzed by immunoblotting with the indicated antibodies. Cell extracts (IN: input) were loaded on lanes 1, 3, 5 and 7, and corresponding immunoprecipitation products were loaded on lanes 2, 4, 6 and 8. (E) Co-purification of endogenous NPC1 in CHO cells with His_6-SKD1 proteins. Upper; intracellular localization of GFP-SKD1. Results shown are the representative images obtained with a confocal microscope. Lower; affinity purification. 0.5% CHAPS extracts were prepared from cells transfected with an empty vector, His_6-SKD1wt or E235Q constructs. His_6-tagged proteins were affinity purified with metal affinity resin and were analyzed by immunoblotting with the indicated antibodies. Cell extracts (IN; input) were loaded on lanes 1, 3 and 5, and corresponding affinity-purification products (AP) were loaded on lanes 2, 4 and 6. (F) In vitro interaction between GST-SKD1 and Flag-NPC1. GST-fused proteins, as shown in the schematic representations, were expressed in *E. coli* and immobilized on glutathione sepharose (left, CBB: Coomassie Blue staining). 0.5% CHAPS extracts (input) were prepared from COS cells expressing Flag-NPC1. Cell extracts were incubated with immobilized GST-fused proteins in the absence or presence of 0.5 mM ADP, ATP or ATPγs. Bound proteins were eluted with glutathione and analyzed by anti-Flag immunoblotting (right). Molecular weights are given on the left (kDa). All results shown are representative and were reproduced at least twice.

(lane 4), whereas no GFP-SKD1wt could be co-precipitated (lane 2). These results were confirmed by probing with anti-SKD1 (lanes 2 and 4). Of note, in addition to GFP-SKD1 at 78 kDa, the anti-SKD1 antibody detected the endogenous SKD1 at 52 kDa (lanes 1, 3, 5 and 7), which, as expected, was not co-precipitated with Flag-NPC1 (lanes 2, 4 and 6). Further confirmation of the results was provided by repeating the above experiments using extracts from cells expressing His_6-tagged SKD1 proteins (data not shown).

Because CHO cells express a readily detectable level of NPC1 (Higaki et al., 2001), we used this cell line to test whether SKD1(E235Q) could interact with endogenous NPC1 (Fig. 4E). Unlike Flag-NPC1 expressed in COS cells, endogenous NPC1 in CHO cells exhibited relatively sharp bands with molecular weights of 170 and 200 kDa. Expression of GFP-SKD1(E235Q), but not GFP-SKD1, again caused the formation of aberrant endosomes containing the mutant protein. These results could be reproduced using His_6-tagged SKD1 proteins (data not shown). When the His_6-tagged SKD1 protein was affinity purified from cell extracts using metal affinity chromatography, a portion of endogenous NPC1 was co-purified with His_6-SKD1(E235Q) (Fig. 4E, lane 6), but not with His_6-SKD1wt (lane 4).

Although the above findings suggested an interaction between NPC1 and the ATP-bound, membrane-associated form of SKD1, it was possible that this interaction was secondary to the formation of the aberrant vesicles that are known to accumulate various endosomal proteins (Yoshimori et al., 2000; Fujita et al., 2003). To address this question, we examined whether NPC1 could bind to SKD1 in vitro (Fig. 4F). Human wt and E235Q mutant SKD1 proteins were expressed as GST-fusion proteins in *Escherichia coli*, whereas Flag-NPC1 was expressed and detergent solubilized from COS cells. GST-SKD1 proteins were immobilized on glutathione sepharose and incubated with 0.5% CHAPS-solubilized cell extracts. Flag-NPC1 bound to the sepharose with binding to both GST-SKD1wt and the E235Q mutant dependent on the presence of ATP or ATPγs. No binding could be detected in the presence of ADP.

Cholesterol depletion facilitated the interaction between NPC1 and wt SKD1

The above findings indicated that NPC1 could interact with the ATP-bound, membrane-associated form of SKD1. To address whether this interaction occurred in cholesterol-depleted cells, cells expressing Flag-NPC1 and His_6-SKD1wt were cultured in cholesterol-depleted medium. In these cells, there was an increase in the amount of His_6-SKD1wt that co-precipitated with Flag-NPC1, as compared with the level in cells cultured in cholesterol-rich medium (Fig. 5A). This co-precipitation was largely suppressed by LDL supplementation of cholesterol-depleted medium.

These findings suggested that at least a part of His_6-SKD1wt was recruited to the endosomes of cholesterol-depleted cells. To confirm this, Opti-prep fractionation of cell homogenates was carried out to detect the membrane-associated form of SKD1 (Fig. 5B). Following fractionation, the endosomal marker protein lamp2 was mainly distributed in fractions 4-7 and cholesterol depletion caused a leftward shift of this distribution to fractions 4-6. Similar to lamp2, Flag-NPC1 was distributed in fractions 3-8 and in 3-7 for the cholesterol-rich

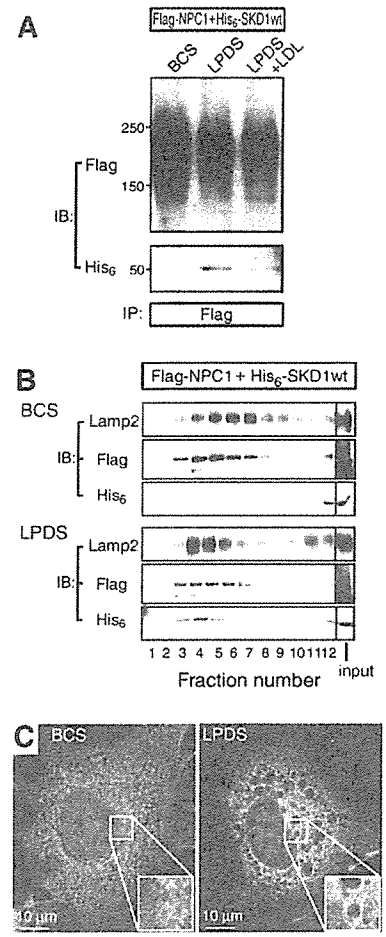

Fig. 5. Effects of cholesterol depletion on an interaction between Flag-NPC1 and wild-type SKD1. Transfected COS cells were cultured in cholesterol-rich or cholesterol-depleted medium with or without LDL for 16 hours. (A) Co-precipitation of His_6-SKD1wt with Flag-NPC1. Cells were transfected with His_6-SKD1wt together with Flag-NPC1 constructs. Anti-Flag immunoprecipitation (IP) products were analyzed by immunoblotting (IB) with the indicated antibodies. Molecular weights are given on the left (kDa). (B) Cell fractionation. Cells were transfected with Flag-NPC1 and His_6-SKD1wt constructs. Membrane fractions (100,000 *g* pellet) of cell homogenates were fractionated on an Opti-prep gradient. The fractions, together with the membrane fractions applied (input), were analyzed by immunoblotting with the indicated antibodies. Shown are representative results that were reproduced three times. (C) Intracellular localization of Flag-NPC1 and GFP-SKD1wt. Cells expressing Flag-NPC1 and GFP-SKD1wt were stained with anti-Flag antibody, and bound antibody was visualized with Alexa Fluor 546-conjugated secondary antibody. Results shown are the representative images obtained with a confocal microscope. Shown in the insets are the enlarged images of the indicated areas.

and cholesterol-depleted cell homogenates, respectively. Cholesterol depletion caused a more significant change in the distribution of His_6-SKD1wt. In cells cultured in cholesterol-rich medium, His_6-SKD1wt was exclusively recovered in the bottom fraction 12, whereas in cells cultured using cholesterol-depleted medium, this protein was also recovered in fractions

3-6. As a control experiment, we examined the distribution of His_6-SKD1(E235Q) and found that this protein was distributed in fractions 3-6 regardless of the cellular cholesterol levels (data not shown).

To confirm the endosomal recruitment of SKD1 in cholesterol-depleted cells further, we examined the intracellular localization of GFP-SKD1wt. As shown in Fig. 4C and Fig. 5C (left panel), when cells expressing Flag-NPC1 and GFP-SKD1wt were cultured in cholesterol-rich medium, GFP-SKD1wt was cytosolic and did not co-localize with endosomal Flag-NPC1. When these cells were cultured in cholesterol-depleted medium, GFP-SKD1wt was concentrated on the rim of enlarged endosomes where it co-localized with Flag-NPC1 (Fig. 5C, right panel).

Cholesterol depletion facilitated ubiquitylation of endogenous NPC1 and its association with SKD1 in controls but not in NPC human skin fibroblasts

The above findings indicated that cholesterol depletion induced ubiquitylation of NPC1 and its interaction with SKD1, when these proteins were expressed in COS cells. To examine whether cholesterol depletion had similar effects on endogenous NPC1 and SKD1, we used primary-cultured human skin fibroblasts from a control subject H34 and an NPC patient UCH (homozygous for the NPC1 H510P mutation). As reported previously (Yamamoto et al., 2000), UCH cells expressed undetectable levels of NPC1 (Fig. 6A), and were included as a negative control. Probing of H34 cell extracts with anti-NPC1 showed that, like CHO cells, these cells contained two species of NPC1 – a major band at 170 kDa and a minor band at 200 kDa – and that cholesterol depletion caused a marginal decrease in the steady-state levels of the NPC1 protein (Fig. 6A). Since immunoprecipitation of the endogenous NPC1 protein was unsuccessful, we employed anti-ubiquitin (P4D1) immunoprecipitation to evaluate the extent of NPC1 ubiquitylation (Fig. 6B). Probing with anti-NPC1 antibody showed that NPC1 was absent in the anti-ubiquitin immunoprecipitation products from cells cultured in cholesterol-rich medium, but was clearly detectable in the immunoprecipitation products from cells depleted of cholesterol. Probing of cell extracts with anti-ubiquitin antibody showed no overall increase of ubiquitylated proteins caused by cholesterol depletion (data not shown). The specificity of anti-NPC1 signals was confirmed by their absence in the immunoprecipitation products from UCH cells. Probing with anti-SKD1 antibody showed that cholesterol depletion increased the level of SKD1 contained in the anti-ubiquitin immunoprecipitation products from H34 cells. By contrast, cholesterol depletion did not alter the levels of SKD1 in the immunoprecipitation products from UCH cells.

Next, using Opti-prep fractionation, the recruitment of SKD1 to the endosomes of cholesterol-depleted cells was examined (Fig. 6C). Both lamp2 and NPC1 in membrane fractions of H34 cells were recovered in fractions 3-5 and, similar to the observations in COS cells (Fig. 5B), cholesterol depletion caused a leftward shift of this distribution to fractions 2 and 3. SKD1 was not recovered in these fractions when cells were cultured in cholesterol-rich medium, but was recovered in fractions 2 and 3 when cells were depleted of cholesterol.

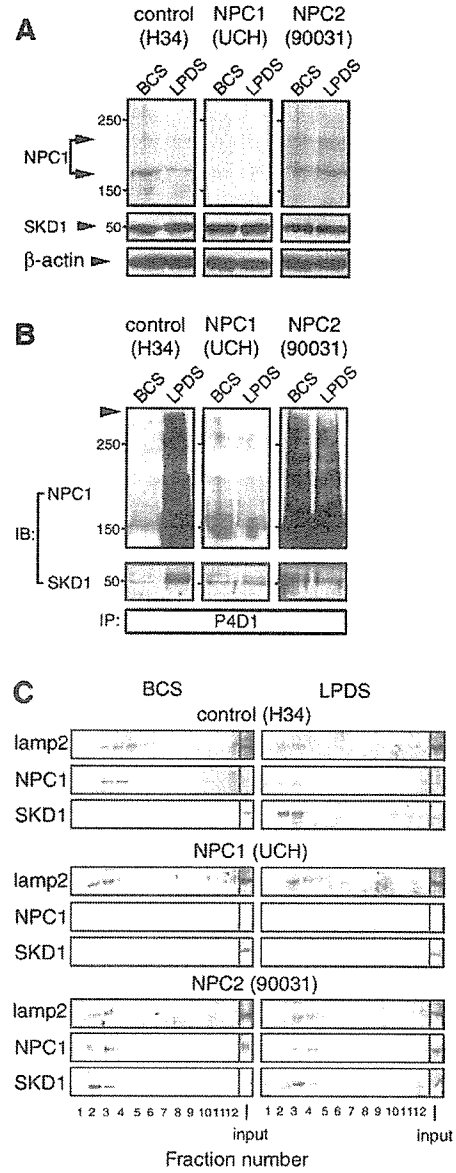

Fig. 6. Effects of cholesterol depletion on ubiquitylation of endogenous NPC1 and its interaction with SKD1 in human skin fibroblasts. Cells from a control subject or patients with NPC1 or NPC2 disease were cultured in cholesterol-rich or cholesterol-depleted medium for 16 hours. (A) Expression of NPC1 and SKD1. 0.5% CHAPS extracts were analyzed by immunoblotting (IB) with antibodies against the indicated proteins. (B) NPC1 ubiquitylation and its association with SKD1. 0.5% CHAPS extracts were subjected to anti-ubiquitin (P4D1) immunoprecipitation (IP) and the immunoprecipitated products were analyzed by immunoblotting with the indicated antibodies. Molecular weights are given on the left (kDa). (C) Cell fractionation. Membrane fractions (100,000 *g* pellet) of cell homogenates were fractionated on an Opti-prep gradient. All results shown are representative and were reproduced at least twice.

In membrane fractions of UCH cells, lamp2 was recovered in fractions 2 and 3 and, unlike in H34 cells, cholesterol depletion caused a rightward shift of this distribution to fractions 3-5. As

expected, NPC1 was absent in UCH cell fractions and, again unlike in H34 cells, SKD1 was not at all recovered in these fractions regardless of the cellular cholesterol levels.

It was possible that this lack of SKD1 recruitment in UCH cells was simply because the cells lacking NPC1 could not be effectively depleted of cholesterol. To address this issue, UCH cells were cultured in cholesterol-depleted medium for 3 days. This treatment abolished endosomal cholesterol accumulation as revealed by filipin staining but again failed to induce endosomal recruitment of SKD1 (data not shown). These findings suggested that the negative results in UCH cells were not a result of ineffective cholesterol depletion, but a result of the absence of NPC1.

Finally, to see if NPC2 is involved in the regulation of NPC1 ubiquitylation, we repeated the same experiments using cells from a patient with NPC2 disease (90031, homozygous for the NPC2 E20X mutation), which lack NPC2 function. Our previous analysis using 0.4% SDS extracts from 100,000 *g* membrane preparations revealed an increased amount of NPC1 in the NPC2 cells as compared with control cells (Millat et al., 2001a). However, anti-NPC1 blotting of 0.5% CHAPS extracts showed comparable levels of NPC1 between H34 and the NPC2 cells (Fig. 6A), suggesting reduced solubility of NPC1 in these cells to this detergent. Nonetheless, anti-ubiquitin immunoprecipitation experiments using the 0.5% CHAPS extracts revealed distinct patterns of NPC1 ubiquitylation. A part of NPC1 was ubiquitylated in these cells regardless of the cholesterol levels (Fig. 6B). This ubiquitylation of NPC1 was accompanied by the presence of SKD1 in the anti-ubiquitin immunoprecipitation products from cells cultured either in cholesterol-rich or cholesterol-depleted medium (Fig. 6B). Opti-prep fractionation of the NPC2 cells showed a distinct distribution pattern of SKD1. Both lamp2 and NPC1 were recovered in fractions 2 and 3 from cells cultured in cholesterol-rich medium and, unlike in H34 cells, cholesterol depletion caused a rightward shift of this distribution to fractions 3-5. In contrast to H34 cells, SKD1 co-localized with NPC1 regardless of the cellular cholesterol levels and it was present in fractions 2 and 3, and in 3-5, from cells cultured in cholesterol-rich and cholesterol-depleted medium, respectively (Fig. 6C). Similar results were obtained by using another NPC2 cell strain 88082 (data not shown), suggesting that they are a common feature of NPC2-deficient cells.

Discussion

The biochemical mechanism and physiological implication of the cholesterol-dependent control of protein ubiquitylation has so far been documented only for HMG-CoAR, a rate-limiting enzyme of cholesterol biosynthesis localized in the ER. Briefly, repletion of cellular cholesterol facilitates association of HMG-CoAR with the Insig proteins, which in turn accelerates its ubiquitylation and proteasomal degradation (Ravid et al., 2000; Sever et al., 2003a; Sever et al., 2003b). We have shown in the current study that ubiquitylation of NPC1 was induced by depletion of cellular cholesterol, but not by its repletion. It is currently unknown how cholesterol exerts opposite effects on NPC1 and HMG-CoAR, the two proteins that share SSDs. These opposite effects possibly result from differences in their subcellular locations and/or the nature of the interacting proteins involved in the regulatory processes. We have shown that two kinds of mutant NPC1 proteins – P691S and δLLNF – failed to respond to cholesterol depletion (Fig. 2). The negative response of the P691S mutant suggested that an intact SSD was required for NPC1 to undergo this modification, whereas the negative response of the δLLNF mutant suggested that the modification took place in the endosomes, where NPC1 normally resides.

Ubiquitylation of a protein can serve as a signal for its degradation or intracellular sorting. Unlike the case of HMG-CoAR, cholesterol-level-dependent NPC1 ubiquitylation does not appear to serve a major role in the control of protein degradation, since cholesterol depletion caused little effect on the steady-state levels of expressed Flag-NPC1 (Fig. 1). Its effect on the steady-state levels of endogenous NPC1 was also marginal (Fig. 6). This finding agrees with the observation by Zhang et al. (Zhang et al., 2001), who found negative effects of cholesterol depletion on the NPC1 protein levels in human skin fibroblasts. Ubiquitylated proteins can be degraded either by the lysosome or by the proteasome in the cytosol. The negative effects of the lysosomal inhibitor leupeptin on ubiquitylation of NPC1 and its steady-state levels (Fig. 3) argue against a role of the lysosome in NPC1 degradation. Our findings with the proteasomal inhibitor MG132 suggest that, like HMG-CoAR, NPC1 does undergo ubiquitylation and proteasomal degradation, but these events appear to be independent to cellular cholesterol levels. MG132 caused accumulation of ubiquitylated Flag-NPC1 and increased its steady-state levels regardless of cellular cholesterol levels (Fig. 3). MG132 induced ubiquitylation of the P691S and δLLNF mutant proteins that failed to respond to cholesterol depletion (Fig. 2). Therefore, as for the role of the proteasome in NPC1 degradation, we hypothesize that NPC1 undergoes ubiquitylation and proteasomal degradation because of protein misfolding, but not because of cholesterol depletion, and that the quality control takes place in the ER, but not in the endosome.

Our findings on the interaction between NPC1 and SKD1 suggest that ubiquitylation of NPC1 induced by cholesterol depletion serves as a sorting signal. The interaction between NPC1 and the ATP-bound, membrane-associated form of SKD1 was indicated by co-localization and co-precipitation of NPC1 and SKD1(E235Q) (Fig. 4C-E). This interaction only occurs with the ATP-bound form of SKD1, as shown by the in vitro binding of NPC1 to immobilized SKD1, which depended on the presence of ATP/ATPγs (Fig. 4F). Importantly, cholesterol depletion induced an interaction between NPC1 and wt SKD1, which presumably was in the ATP-bound, membrane-associated form (Fig. 5). The effect of cholesterol depletion on NPC1 ubiquitylation was also demonstrated for the endogenous protein in human skin fibroblasts (Fig. 6B) and, again, this ubiquitylation was accompanied by recruitment of SKD1 to the endosomal fractions (Fig. 6C). In yeast, Vps4 is required for disassembly of the ESCRT-III, which contains other Vps proteins Vps2, Vps20, Vps24 and Vps32/Snf7 (Babst et al., 2002a). Mammalian counterparts to these proteins have recently been identified (Fujita et al., 2004; Peck et al., 2004; Yan et al., 2005). Our findings suggest that NPC1 interacted with these proteins in the presence of SKD1(E235Q) or in cells depleted of cholesterol.

Two lines of questions can be addressed regarding the interaction between NPC1 and the ESCRT complex. First, how is ubiquitylated NPC1 recognized by the ESCRT complex?

Tsg101 is a mammalian ortholog of yeast Vps23 and has been shown to bind directly to ubiquitylated EGFR (Bishop and Woodman, 2001; Bishop et al., 2002). We tested whether Flag-NPC1 interacted with endogenous Tsg101 in COS cells, but could not detect any interaction between these two proteins. Therefore, it is likely that NPC1 is recognized by the ESCRT complex in a manner that is different to EGFR. Second, what is the role of the ESCRT complex in the intracellular sorting of NPC1? NPC1 is primarily localized on the late endosome and can transiently associate with cholesterol-enriched lysosomes (Higgins et al., 1999). The ESCRT complex plays a crucial role in the sorting of ubiquitylated proteins form the endosome to the lysosome through multivesicular bodies (Bishop and Woodman, 2000; Yoshimori et al., 2000; Bishop et al., 2002; Fujita et al., 2003) and, in Vps mutant yeast cells, Ncr1 is trapped in the pre-vacuolar compartments (Zhang et al., 2004), which correspond to mammalian endosomes. Therefore, it is likely that the ESCRT complex is required for the sorting of NPC1 from the late endosome to the lysosome. At least in yeast, it has been shown that the entry of the ubiquitylated protein to multivesicular bodies is preceded by de-ubiquitylation of the protein (Babst et al., 2002a). Given the effects of cholesterol depletion, we propose that the sorting of NPC1 is regulated by the local cholesterol content of the endosomal membrane. When it is low, NPC1 is ubiquitylated and is associated with the ESCRT complex. Its entry into multivesicular bodies and subsequent delivery to the lysosome might be triggered by cholesterol feeding, which presumably induces de-ubiquitylation of the protein. This sorting might be an obligatory step for the NPC1 function to relocate LDL-derived lysosomal cholesterol; further analysis is required to test our hypothesis.

Finally, our findings regarding the NPC2 cells provided an important insight into a functional relationship between NPC1 and NPC2. In cells that lack functional NPC2, ubiquitylation of NPC1 (Fig. 6B) and endosomal recruitment of SKD1 (Fig. 6C) occurred under cholesterol-rich conditions, similar to the results obtained in control cells depleted of cholesterol. Thus, under cholesterol-rich conditions, the presence of functional NPC2 was required to prevent NPC1 ubiquitylation and subsequent association with SKD1. NPC2 contains an MD-2-like lipid-recognition domain and binds cholesterol. By analogy to other proteins that contain this domain, it can be postulated that NPC2 extracts membrane-embedded cholesterol and makes it available to other proteins (Inohara and Nunez, 2002). Therefore, one possible explanation for NPC1 ubiquitylation in NPC2 cells is that cholesterol is unavailable to the membrane domains where NPC1 resides, inducing NPC1 modification that normally takes place under conditions of cholesterol deprivation. This explanation is consistent with the increased protein levels of NPC1 in NPC2 cells (Millat et al., 2001a), given that NPC1 ubiquitylation caused by cholesterol depletion does not lead to its degradation. Alternatively, it is also possible that NPC2 deficiency acts indirectly, by inducing aberrant compartmentalization of NPC1, and triggering its ubiquitylation. However, this alternative explanation does not agree with our observation that U18666A, which induces aberrant compartmentalization of NPC1, failed to affect its ubiquitylation (Fig. 1F). We suggest that cholesterol-level-dependent ubiquitylation of NPC1 is a crucial event not only to understand the intracellular sorting of NPC1 but also to unravel the functional relationship between NPC1 and NPC2 in future studies.

Materials and Methods

Materials

Dulbecco's modified Eagle's medium (DMEM), Ham's F12 medium and LipofectAMINE reagent were from Life Technologies. Bovine calf serum (BCS) was from Atlanta Biologicals. Bovine lipoprotein-deficient serum (LPDS), human LDL, anti-Flag M2 agarose and rabbit polyclonal anti-Flag antibody were from Sigma. Rabbit polyclonal anti-NPC1 antibody and mouse monoclonal antibodies against ubiquitin (P4D1), myc, His_6 and GFP were from Santa Cruz Biotech. Rabbit polyclonal anti-SKD1 has been described (Yoshimori et al., 2000).

Mammalian expression of recombinant proteins

pASC9/Flag-NPC1, an expression plasmid for human NPC1 with a Flag tag inserted in the *ClaI* site, has been described (Davies and Ioannou, 2000). pSV-SPORT/NPC1 wild-type (wt) and the P691S mutant were a gift from J. F. Strauss III (Department of Obstetrics and Gynecology, University of Pennsylvania School of Medicine, VA). The *PsyI* fragment of the Flag-NPC1 cDNA that flanks the Flag epitope was introduced to the corresponding site of pSV-SPORT/NPC1 wt and P691S to generate a Flag-tagged version of the cDNAs. The C-terminal 12 bp were deleted from pSV-SPORT/Flag-NPC1 by PCR-based mutagenesis to generate a cDNA that encoded Flag-NPC1(δLLNF). An expression plasmid for myc/His_6-tagged yeast ubiquitin was a gift from R. Kopito (Department of Biological sciences, Stanford University, CA). Expression plasmids for GFP-tagged mouse wt and E235Q mutant SKD1 have been described (Yoshimori et al., 2000). The entire coding sequence of human SKD1 cDNA (Vps4-B) (Scheuring et al., 2001) was obtained by RT-PCR with primers 5′-TCCGCCATGTCATCCACTTCG-3′ and 5′-GCTTTTGGCTTAG-CCTTCTTG-3′ from human skin fibroblasts cDNA. A His_6 epitope was introduced at the C-terminus by PCR and the cDNA was subcloned to the *EcoRI/XhoI* site of a mammalian expression vector pME18sf. An amino acid substitution E235Q was introduced to pME/His_6-SKD1 using a Quick Change Site-Directed mutagenesis kit (Stratagene) and was confirmed by direct sequencing. Cells were transfected using LipofectAMINE reagent according to the manufacturer's instructions.

Cell culture

COS cells and human skin fibroblasts were maintained in DMEM/10% BCS at 37°C in a humidified atmosphere containing 5% CO_2. Human skin fibroblasts were from a control human subject (H34), and from patients with NPC1 (UCH) (Yamamoto et al., 2000) and NPC2 (90031 and 88082) (Millat et al., 2001b) diseases. CHO cells were maintained in F12 medium as above. To deplete cellular cholesterol, cells were cultured for the time indicated in 10% LPDS supplemented with an HMG-CoAR inhibitor compactin (2 μM) and sodium mevalonate (0.1 mM), which assures cell viability (Ravid et al., 2000). Where indicated, this cholesterol-depleted medium was supplemented with 20 μg/ml LDL. For determination of cholesterol levels, cells in 6-well plates were scraped into PBS and lysed by sonication. Concentrations of protein and total cholesterol in the lysates were determined by using the microprotein assay kit (BioRad) and the Amplex red cholesterol assay kit (Molecular Probes), respectively, according to the manufacturer's instructions.

Immunoprecipitation and affinity purification

All procedures were carried out at 4°C. Cells were washed with PBS and lysed by sonication in buffer A [Tris-HCl 10 mM pH 7.4, NaCl 150 mM, 1 mM EDTA, 1 mM EGTA, 0.5% CHAPS and a protease inhibitor cocktail (Boehringer)]. After a brief centrifugation to remove insoluble material, the supernatant was precleared with an aliquot of agarose beads. For immunoprecipitation of Flag-NPC1, the extracts were incubated for 16 hours with anti-Flag M2 agarose beads, washed with buffer A, followed by elution of bound proteins by heating at 65°C for 10 minutes in SDS-PAGE sample buffer. SDS-PAGE, western transfer and immunoblotting were carried out as previously described (Sugimoto et al., 2001). The blot was developed using an ECL kit (Amersham Pharmacia). For immunoprecipitation of ubiquitylated proteins, cell extracts were incubated with anti-ubiquitin P4D1 antibodies for 16 hours and the immunoprecipitates were collected with protein A sepharose. For affinity purification of His_6-tagged proteins (myc/His_6-ubiquitin or His_6-SKD1), cell extracts were incubated for 16 hours with TALON metal affinity resin (Clontech). Bound proteins were analyzed as described above.

Cell fractionation

Cells were harvested in Tris-buffered saline (TBS; Tris-HCl 10 mM pH 7.4, NaCl 150 mM) supplemented with a protease inhibitor cocktail and lysed by sonication. The cell lysates were incubated on ice for 30 minutes in TBS supplemented with 1% Triton X-100 and 0.1% SDS to give total extracts. To prepare 1% Triton X-100-soluble and Triton X-100-insoluble fractions, the cell lysates were incubated in TBS + 1% Triton X-100 and, after centrifugation at 100,000 *g* for 30 minutes, the pellet was suspended in TBS + 1% Triton X-100 + 0.1% SDS. For subcellular fractionation, membranes were fractionated by using an Opti-prep gradient (Axis-

Shield) as described (Lin et al., 2004). Briefly, cells were homogenized with a potter homogenizer in ice-cold buffer (Hepes 10 mM pH 7.0, 1 mM EDTA, 1 mM EGTA supplemented with a protease inhibitor cocktail). After centrifugation at 100,000 *g* for 1 hour at 4°C, the supernatant was discarded and the pellet was resuspended in the same buffer, overlaid onto an Opti-prep gradient and centrifuged at 100,000 *g* for 16 hours at 4°C. The top 12 fractions of the gradient were recovered and numbered accordingly.

Immunofluorescence

All procedures were carried out at room temperature. Cells were fixed for 2 minutes with acetone:methanol (1:1 v/v) and incubated for 30 minutes in PBS + 1% bovine serum albumin (BSA). They were then incubated for 1 hour with anti-Flag antibody or anti-His_6 antibody in PBS + 1% BSA. Bound antibodies were visualized with an Alexa Fluor 546-conjugated secondary antibody and images were obtained using a BioRad MRC1024 confocal laser-scanning microscope.

Bacterial expression of GST-SKD1 and in vitro binding assays

The *EcoRI*/*XhoI* fragment of pME/SKD1 was transferred to pGEX-6P (Amersham Pharmacia). DH5α competent cells were transformed with the plasmid and protein expression was induced with 1 mM IPTG at 37°C for 3 hours. GST-SKD1 was recovered from bacterial pellets in 8 M urea, dialyzed against TBS and immobilized on glutathione sepharose. For in vitro binding assays, GST-SKD1 glutathione sepharose was incubated with 0.5% CHAPS extracts from Flag-NPC1-expressing cells at 4°C for 2 hours, in the absence or presence of ADP, ATP or ATPγs (all at 0.5 mM). The sepharose resin was washed with TBS + 0.5% CHAPS and bound proteins were eluted with glutathione and analyzed by SDS-PAGE followed by immunoblotting with anti-Flag antibody.

We thank J. F. Strauss III for mutant NPC1 cDNAs and R. Kopito for ubiquitin cDNA. This work was supported in part by a Grant-in-Aid for Scientific Research from the Ministry of Education, Culture, Sports, Science and Technology of Japan.

References

Babst, M., Sato, T. K., Banta, L. M. and Emr, S. D. (1997). Endosomal transport function in yeast requires a novel AAA-type ATPase, Vps4p. *EMBO J.* **16**, 1820-1831.

Babst, M., Wendland, B., Estepa, E. J. and Emr, S. D. (1998). The Vps4p AAA ATPase regulates membrane association of a Vps protein complex required for normal endosome function. *EMBO J.* **17**, 2982-2993.

Babst, M., Katzmann, D. J., Estepa-Sabal, E. J., Meerloo, T. and Emr, S. D. (2002a). ESCRT-III: an endosome-associated heterooligomeric protein complex required for MVB sorting. *Dev. Cell* **3**, 271-282.

Babst, M., Katzmann, D. J., Snyder, W. B., Wendland, B. and Emr, S. D. (2002b). Endosome-associated complex, ESCRT-II, recruits transport machinery for protein sorting at the multivesicular body. *Dev. Cell* **3**, 283-289.

Berger, A. C., Hanson, P. K., Wylie Nichols, J. and Corbett, A. H. (2005). A yeast model system for functional analysis of the niemann-pick type C protein 1 homolog, ncr1p. *Traffic* **6**, 907-917.

Bishop, N. and Woodman, P. (2000). ATPase-defective mammalian VPS4 localizes to aberrant endosomes and impairs cholesterol trafficking. *Mol. Biol. Cell* **11**, 227-239.

Bishop, N. and Woodman, P. (2001). TSG101/mammalian VPS23 and mammalian VPS28 interact directly and are recruited to VPS4-induced endosomes. *J. Biol. Chem.* **276**, 11735-11742.

Bishop, N., Horman, A. and Woodman, P. (2002). Mammalian class E vps proteins recognize ubiquitin and act in the removal of endosomal protein-ubiquitin conjugates. *J. Cell Biol.* **157**, 91-101.

Carstea, E. D., Morris, J. A., Coleman, K. G., Loftus, S. K., Zhang, D., Cummings, C., Gu, J., Rosenfeld, M., Pavan, W. J., Krizman, D. B. et al. (1997). Niemann-Pick C1 disease gene: homology to mediators of cholesterol homeostasis. *Science* **277**, 228-231.

Davies, J. P. and Ioannou, Y. A. (2000). Topological analysis of Niemann-Pick C1 protein reveals that the membrane orientation of the putative sterol-sensing domain is identical to those of 3-hydroxy-3-methylglutaryl-CoA reductase and sterol regulatory element binding protein cleavage-activating protein. *J. Biol. Chem.* **275**, 24367-24374.

Davies, J. P., Chen, F. W. and Ioannou, Y. A. (2000). Transmembrane molecular pump activity of Niemann-Pick C1 protein. *Science* **290**, 2295-2298.

Fujita, H., Yamanaka, M., Imamura, K., Tanaka, Y., Nara, A., Yoshimori, T., Yokota, S. and Himeno, M. (2003). A dominant negative form of the AAA ATPase SKD1/VPS4 impairs membrane trafficking out of endosomal/lysosomal compartments: class E vps phenotype in mammalian cells. *J. Cell Sci.* **116**, 401-414.

Fujita, H., Umezuki, Y., Imamura, K., Ishikawa, D., Uchimura, S., Nara, A., Yoshimori, T., Hayashizaki, Y., Kawai, J., Ishidoh, K. et al. (2004). Mammalian class E Vps proteins, SBP1 and mVps2/CHMP2A, interact with and regulate the function of an AAA-ATPase SKD1/Vps4B. *J. Cell Sci.* **117**, 2997-3009.

Garver, W. S., Heidenreich, R. A., Erickson, R. P., Thomas, M. A. and Wilson, J. M. (2000). Localization of the murine Niemann-Pick C1 protein to two distinct intracellular compartments. *J. Lipid Res.* **41**, 673-687.

Hicke, L. (2001). A new ticket for entry into budding vesicles-ubiquitin. *Cell* **106**, 527-530.

Higaki, K., Ninomiya, H., Sugimoto, Y., Suzuki, T., Taniguchi, M., Niwa, H., Pentchev, P. G., Vanier, M. T. and Ohno, K. (2001). Isolation of NPC1-deficient Chinese hamster ovary cell mutants by gene trap mutagenesis. *J. Biochem.* **129**, 875-880.

Higgins, M. E., Davies, J. P., Chen, F. W. and Ioannou, Y. A. (1999). Niemann-Pick C1 is a late endosome-resident protein that transiently associates with lysosomes and the trans-Golgi network. *Mol. Genet. Metab.* **68**, 1-13.

Inohara, N. and Nunez, G. (2002). ML – a conserved domain involved in innate immunity and lipid metabolism. *Trends Biochem. Sci.* **27**, 219-221.

Katzmann, D. J., Babst, M. and Emr, S. D. (2001). Ubiquitin-dependent sorting into the multivesicular body pathway requires the function of a conserved endosomal protein sorting complex, ESCRT-I. *Cell* **106**, 145-155.

Ko, D. C., Gordon, M. D., Jin, J. Y. and Scott, M. P. (2001). Dynamic movements of organelles containing Niemann-Pick C1 protein: NPC1 involvement in late endocytic events. *Mol. Biol. Cell* **12**, 601-614.

Lin, H., Sugimoto, Y., Ohsaki, Y., Ninomiya, H., Oka, A., Taniguchi, M., Ida, H., Eto, Y., Ogawa, S., Matsuzaki, Y. et al. (2004). N-octyl-beta-valienamine up-regulates activity of F213I mutant beta-glucosidase in cultured cells: a potential chemical chaperone therapy for Gaucher disease. *Biochim. Biophys. Acta* **1689**, 219-228.

Millard, E. E., Gale, S. E., Dudley, N., Zhang, J., Schaffer, J. E. and Ory, D. S. (2005). The sterol-sensing domain of the Niemann-Pick C1 (NPC1) protein regulates trafficking of low density lipoprotein cholesterol. *J. Biol. Chem.* **280**, 28581-28590.

Millat, G., Marcais, C., Tomasetto, C., Chikh, K., Fensom, A. H., Harzer, K., Wenger, D. A., Ohno, K. and Vanier, M. T. (2001a). Niemann-Pick C1 disease: correlations between NPC1 mutations, levels of NPC1 protein, and phenotypes emphasize the functional significance of the putative sterol-sensing domain and of the cysteine-rich luminal loop. *Am. J. Hum. Genet.* **68**, 1373-1385.

Millat, G., Chikh, K., Naureckiene, S., Sleat, D. E., Fensom, A. H., Higaki, K., Elleder, M., Lobel, P. and Vanier, M. T. (2001b). Niemann-Pick disease type C: spectrum of HE1 mutations and genotype/phenotype correlations in the NPC2 group. *Am. J. Hum. Genet.* **69**, 1013-1021.

Naureckiene, S., Sleat, D. E., Lackland, H., Fensom, A., Vanier, M. T., Wattiaux, R., Jadot, M. and Lobel, P. (2000). Identification of HE1 as the second gene of Niemann-Pick C disease. *Science* **290**, 2298-2301.

Patterson, M. C., Vanier, M. T., Suzuki, K., Morris, J. A., Carstea, E. D., Neufeld, E. B., Blanchette-Mackie, E. J. and Pentchev, P. G. (2001). Niemann-Pick disease type C: a lipid trafficking disorder. In *The Metabolic and Molecular Bases of Inherited Disease* (ed. C. R. Scriver, A. L. Beaudet, W. S. Sly, D. Valle, B. Childs, K. W. Kinzler and B. Vogelstein), pp. 3611-3634. New York: McGraw Hill.

Peck, J. W., Bowden, E. T. and Burbelo, P. D. (2004). Structure and function of human Vps20 and Snf7 proteins. *Biochem. J.* **377**, 693-700.

Ravid, T., Doolman, R., Avner, R., Harats, D. and Roitelman, J. (2000). The ubiquitin-proteasome pathway mediates the regulated degradation of mammalian 3-hydroxy-3-methylglutaryl-coenzyme A reductase. *J. Biol. Chem.* **275**, 35840-35847.

Scheuring, S., Rohricht, R. A., Schoning-Burkhardt, B., Beyer, A., Muller, S., Abts, H. F. and Kohrer, K. (2001). Mammalian cells express two VPS4 proteins both of which are involved in intracellular protein trafficking. *J. Mol. Biol.* **312**, 469-480.

Scott, C., Higgins, M. E., Davies, J. P. and Ioannou, Y. A. (2004). Targeting of NPC1 to late endosomes involves multiple signals, including one residing within the putative sterol-sensing domain. *J. Biol. Chem.* **279**, 48214-48223.

Sever, N., Song, B. L., Yabe, D., Goldstein, J. L., Brown, M. S. and DeBose-Boyd, R. A. (2003a). Insig-dependent ubiquitination and degradation of mammalian 3-hydroxy-3-methylglutaryl-CoA reductase stimulated by sterols and geranylgeraniol. *J. Biol. Chem.* **278**, 52479-52490.

Sever, N., Yang, T., Brown, M. S., Goldstein, J. L. and DeBose-Boyd, R. A. (2003b). Accelerated degradation of HMG CoA reductase mediated by binding of insig-1 to its sterol-sensing domain. *Mol. Cell* **11**, 25-33.

Sharma, M., Pampinella, F., Nemes, C., Benharouga, M., So, J., Du, K., Bache, K. G., Papsin, B., Zerangue, N., Stenmark, H. et al. (2004). Misfolding diverts CFTR from recycling to degradation: quality control at early endosomes. *J. Cell Biol.* **164**, 923-933.

Shenoy, S. K., McDonald, P. H., Kohout, T. A. and Lefkowitz, R. J. (2001). Regulation of receptor fate by ubiquitination of activated beta 2-adrenergic receptor and beta-arrestin. *Science* **294**, 1307-1313.

Simons, K. and Ikonen, E. (1997). Functional rafts in cell membranes. *Nature* **387**, 569-572.

Sleat, D. E., Wiseman, J. A., El-Banna, M., Price, S. M., Verot, L., Shen, M. M., Tint, G. S., Vanier, M. T., Walkley, S. U. and Lobel, P. (2004). Genetic evidence for nonredundant functional cooperativity between NPC1 and NPC2 in lipid transport. *Proc. Natl. Acad. Sci. USA* **101**, 5886-5891.

Sugimoto, Y., Ninomiya, H., Ohsaki, Y., Higaki, K., Davies, J. P., Ioannou, Y. A. and Ohno, K. (2001). Accumulation of cholera toxin and GM1 ganglioside in the early endosome of Niemann-Pick C1-deficient cells. *Proc. Natl. Acad. Sci. USA* **98**, 12391-12396.

Vanier, M. T. and Millat, G. (2004). Structure and function of the NPC2 protein. *Biochim. Biophys. Acta* **1685**, 14-21.

Watari, H., Blanchette-Mackie, E. J., Dwyer, N. K., Watari, M., Neufeld, E. B., Patel, S., Pentchev, P. G. and Strauss, J. F., III (1999a). Mutations in the leucine zipper motif and sterol-sensing domain inactivate the Niemann-Pick C1 glycoprotein. *J. Biol. Chem.* **274**, 21861-21866.

Watari, H., Blanchette-Mackie, E. J., Dwyer, N. K., Glick, J. M., Patel, S., Neufeld, E. B., Brady, R. O., Pentchev, P. G. and Strauss, J. F., III (1999b). Niemann-Pick

C1 protein: obligatory roles for N-terminal domains and lysosomal targeting in cholesterol mobilization. *Proc. Natl. Acad. Sci. USA* **96**, 805-810.

Yabe, D., Brown, M. S. and Goldstein, J. L. (2002). Insig-2, a second endoplasmic reticulum protein that binds SCAP and blocks export of sterol regulatory element-binding proteins. *Proc. Natl. Acad. Sci. USA* **99**, 12753-12758.

Yamamoto, T., Ninomiya, H., Matsumoto, M., Ohta, Y., Nanba, E., Tsutsumi, Y., Yamakawa, K., Millat, G., Vanier, M. T., Pentchev, P. G. et al. (2000). Genotype-phenotype relationship of Niemann-Pick disease type C: a possible correlation between clinical onset and levels of NPC1 protein in isolated skin fibroblasts. *J. Med. Genet.* **37**, 707-712.

Yan, Q., Hunt, P. R., Frelin, L., Vida, T. A., Pevsner, J. and Bean, A. J. (2005). mVps24p functions in EGF receptor sorting/trafficking from the early endosome. *Exp. Cell Res.* **304**, 265-273.

Yang, T., Espenshade, P. J., Wright, M. E., Yabe, D., Gong, Y., Aebersold, R., Goldstein, J. L. and Brown, M. S. (2002). Crucial step in cholesterol homeostasis: sterols promote binding of SCAP to INSIG-1, a membrane protein that facilitates retention of SREBPs in ER. *Cell* **110**, 489-500.

Yoshimori, T., Yamagata, F., Yamamoto, A., Mizushima, N., Kabeya, Y., Nara, A., Miwako, I., Ohashi, M., Ohsumi, M. and Ohsumi, Y. (2000). The mouse SKD1, a homologue of yeast Vps4p, is required for normal endosomal trafficking and morphology in mammalian cells. *Mol. Biol. Cell* **11**, 747-763.

Zhang, M., Dwyer, N. K., Neufeld, E. B., Love, D. C., Cooney, A., Comly, M., Patel, S., Watari, H., Strauss, J. F., III, Pentchev, P. G. et al. (2001). Sterol-modulated glycolipid sorting occurs in niemann-pick C1 late endosomes. *J. Biol. Chem.* **276**, 3417-3425.

Zhang, S., Ren, J., Li, H., Zhang, Q., Armstrong, J. S., Munn, A. L. and Yang, H. (2004). Ncr1p, the yeast ortholog of mammalian Niemann Pick C1 protein, is dispensable for endocytic transport. *Traffic* **5**, 1017-1030.

Journal of Cell Science

主なミトコンドリア脳筋症

電子伝達系異常症

杉江 秀夫　杉江 陽子

ミトコンドリア電子伝達系

ミトコンドリアは細胞内に存在する小器官で，嫌気性解糖の段階で1モルのグルコースから2モルのATPが産生されるのに対し，ミトコンドリア電子伝達系では36モルのATPが産生され，生体で必要なエネルギーの必要量の大部分の産生を担っている．ミトコンドリア内膜に局在している電子伝達系は，電子を内膜に伝達させて，水素イオン(H^+)をintermembrane space(膜間腔)に輸送し(電子伝達系)，生じるH^+濃度勾配(電位差，pH差)を用いて，最終段階で共役的にATPの合成を行う(酸化的リン酸化)．これらの過程をミトコンドリア呼吸鎖 mitochondrial respiratory chainと呼ぶ[1,2]．図1にミトコンドリア呼吸鎖の構成を示す．ミトコンドリア呼吸鎖は，複合体I (NADH-ubiquinone oxidoreductase)，II (SDH-ubiquinone oxidoreductase)，III (ubiquinone-cytochrome *c* oxidoreductase)，IV (cytochrome *c* oxidase：COX)と呼ばれる4つの複合体蛋白から構成され，ミトコンドリア内膜に局在している．最終的にATP合成酵素(複合体V)でATPの合成が行われる．ミトコンドリア呼吸鎖のI-Vの複合体の他にさらに3つの蛋白が電子伝達には必要である．それらはdihydroorotate-CoQ oxidoreductase (DHO-QO)，electron transfer flavoprotein-CoQ oxidoreductase (ETF-QO)，adenosine nucleotide translocator (ANT)である(表1)．ミトコンドリアの内膜にはその他coenzyme Q (CoQ，ユビキノン)，チトクローム *c* があり，CoQは内膜内を自由に動きまわり，電子を伝達したりH^+を膜間腔に汲み出す働きをしている．哺乳類では，ATPの80～90%は，ミトコンドリアでの酸化的リン酸化により生成されるが，一方ミトコンドリアはATPを合成して細胞の生を維持するだけでなく，アポトーシスにも関与し細胞の維持に

すぎえ ひでお　浜松市発達医療総合センター所長/小児神経科
すぎえ ようこ　浜松市発達医療総合センター/小児神経科

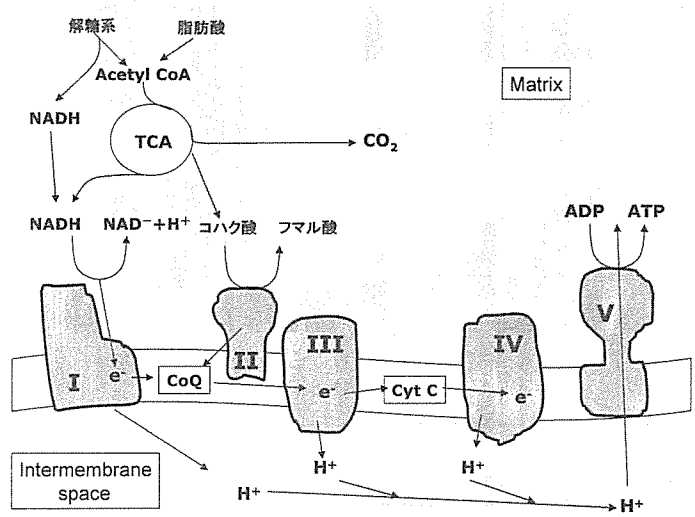

図1　ミトコンドリア呼吸鎖の構成

表1　ミトコンドリア呼吸鎖の構成

	複合体I	複合体II	複合体III	複合体IV	複合体V	DHO-QO	ETF-QO	ANT
酵　素	NADH-ubiquinone oxidoreductase	SDH-ubiquinone oxidoreductase	Ubiquinone-cytochrome *c* oxidoreductase	Cytochrome *c* oxidase	ATP synthase	Dihydroorotate-CoQ oxidoreductase	Electron transfer flavoprotein-CoQ oxidoreductase	Adenosine nucleotide translocator
サブユニット								
nDNA	43	4	10	10	14	1	1	1
mtDNA	7	0	1	3	2	0	0	0

0289-0585/06/¥500/論文/JCLS

大きな役割を果たしている.

複合体と遺伝子

複合体は表1に示すように複合体IIを除き，ミトコンドリアDNA(mtDNA)と核DNA(nDNA)の両者にコードされる複数のサブユニットから構成されている．従ってミトコンドリア病の遺伝は，mtDNAの異常に起因すれば母系遺伝を示すが，nDNAの異常であればMendel遺伝形式をとる．しかしmtDNAの巨大欠失によるものはほとんどが孤発例である．また最近父親由来のmtDNAが遺伝している例も報告され[3]，今後さらにその点の解明が必要である．一般的な臨床の場面では，pedigreeで男女ともに罹患し，母親から疾患が経由している家系ではミトコンドリア病，特にmtDNAの点変異が疑われる[4]．

筋生検と複合体の検索

一般的にミトコンドリア病はmultisystemicな症状を呈するが，脳，筋，心筋はその中でも障害を受けやすい臓器である．そのため原因検索には筋生検を用いて，組織化学，電顕，生化学検査が行われることが多い．ragged-red fiber (RRF)(図2)は筋組織化学的にミトコンドリア異常の重要な目安で，ミトコンドリア異常症の70～80%にみられる．しかしすべてのミトコンドリア異常症に認められる変化ではない．特にnDNAの変異によると考えられる疾患ではRRFはほとんど出現しない．電子伝達系疾患の診断では生体試料として骨格筋，線維芽細胞，リンパ球などで複合体酵素活性が測定される．複合体の酵素は解糖系の酵素と異なり，酵素活性が筋の保存状態に左右され不安定であり，また病気の進行や加齢などによっても二次的に低値を示す例があるので，活性値を論ずるには様々な条件について考慮しながら解釈することが必要である[5]．一般に，複合体I＋III，II＋IIIでの活性低下がみられた場合はCoQの異常，また複合体I，II，III，およびaconitaseのすべてが低下している場合はiron sulfur proteinの異常，複合体I，II，III，IVすべての異常であれば核成分のミトコンドリアへの移送障害，またはmtDNAの欠乏，複合体I，IV欠損であればmtDNAの点変異，欠失などを疑うことができる[6]．

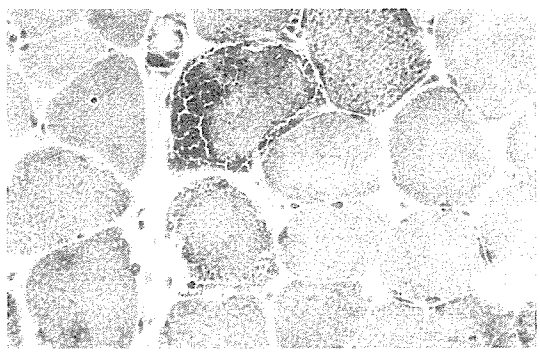

図2　MELAS患者における ragged-red fiber
Gomori-トリクローム染色.

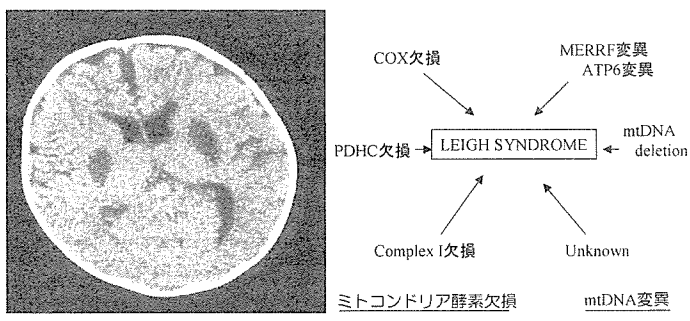

図3　Leigh脳症
A）頭部CT所見．両側基底核の低吸収が認められる．
B）原因の多様性.

複合体酵素欠損と症状の発現

ミトコンドリア病の発症頻度は約10～15/100,000人といわれているが，症状発現には幅広いスペクトラムがあるため，実際の罹患率はもう少し多いのではないかと考えられる．またミトコンドリア病の発症には特有の病態がある．つまり，異常mtDNA(mutant mtDNA)は正常mtDNA(wild mtDNA)とさまざまな割合で細胞，臓器に分布している(heteroplasmy)ため，症状に多様性が認められる．また，発症に至るには，異常ミトコンドリアがどの程度の比率でその細胞，臓器に存在しているのかが重要で，異常mtDNAの占める比率がある閾値を超えた場合に発症につながると考えられる(threshold effect)．したがって異常ミトコンドリアを有していても閾値以下であれば無症状であったり，軽症であったりと症状の軽重，性質は広いスペクトラムを呈することとなる．ミトコンドリアはubiquitousに存在しているが，ある臓器に特異的に異常ミトコンドリアが偏在する(skewed heteroplasmy)[7]場合があり，臓器特異的な症状を示すこととなる．

ミトコンドリア病のもう一つの特徴として，異なる遺伝子異常でありながら同一の疾患の病像を呈したり，一つの遺伝子異常でありながら，示す病像が多様であったりする．